UPPSALA
UNIVERSITET

Digital Comprehensive Summaries of Uppsala Dissertations from the Faculty of Science and Technology 717

Cadmium Free Buffer Layers and the Influence of their Material Properties on the Perfomance of $Cu(In,Ga)Se_2$ Solar Cells

ADAM HULTQVIST

ACTA
UNIVERSITATIS
UPSALIENSIS
UPPSALA
2010

ISSN 1651-6214
ISBN 978-91-554-7944-2
urn:nbn:se:uu:diva-133112

Dissertation presented at Uppsala University to be publicly examined in Häggsalen, Ångströmlaboratoriet, Lägerhyddsvägen 1, Uppsala, Thursday, December 16, 2010 at 13:00 for the degree of Doctor of Philosophy. The examination will be conducted in English.

Abstract
Hultqvist, A. 2010. Cadmium Free Buffer Layers and the Influence of their Material Properties on the Perfomance of Cu(In,Ga)Se_2 Solar Cells. Acta Universitatis Upsaliensis. *Digital Comprehensive Summaries of Uppsala Dissertations from the Faculty of Science and Technology* 717. 75 pp. Uppsala. ISBN 978-91-554-7944-2.

CdS is conventionally used as a buffer layer in Cu(In,Ga)Se_2, CIGS, solar cells. The aim of this thesis is to substitute CdS with cadmium-free, more transparent and environmentally benign alternative buffer layers and to analyze how the material properties of alternative layers affect the solar cell performance. The alternative buffer layers have been deposited using Atomic Layer Deposition, ALD. A theoretical explanation for the success of CdS is that its conduction band, E_c, forms a small positive offset with that of CIGS.

In one of the studies in this thesis the theory is tested experimentally by changing both the E_c position of the CIGS and of Zn(O,S) buffer layers through changing their gallium and sulfur contents respectively. Surprisingly, the top performing solar cells for all gallium contents have Zn(O,S) buffer layers with the same sulfur content and properties in spite of predicted unfavorable E_c offsets. An explanation is proposed based on observed non-homogenous composition in the buffer layer.

This thesis also shows that the solar cell performance is strongly related to the resistivity of alternative buffer layers made of (Zn,Mg)O. A tentative explanation is that a high resistivity reduces the influence of shunt paths at the buffer layer/absorber interface. For devices in operation however, it seems beneficial to induce persistent photoconductivity, by light soaking, which can reduce the effective E_c barrier at the interface and thereby improve the fill factor of the solar cells.

Zn-Sn-O is introduced as a new buffer layer in this thesis. The initial studies show that solar cells with Zn-Sn-O buffer layers have comparable performance to the CdS reference devices.

While an intrinsic ZnO layer is required for a high reproducibility and performance of solar cells with CdS buffer layers it is shown in this thesis that it can be thinned if Zn(O,S) or omitted if (Zn,Mg)O buffer layers are used instead. As a result, a top conversion efficiency of 18.1 % was achieved with an (Zn,Mg)O buffer layer, a record for a cadmium and sulfur free CIGS solar cell.

Keywords: Cu(In, Ga)Se2, Solar cells, Thin film, Buffer layer, Window layer, ZnO, Zn(O, S), (Zn, Mg)O, Zn-Sn-O

Adam Hultqvist, Department of Engineering Sciences, Solid State Electronics, Box 534, Uppsala University, SE-75121 Uppsala, Sweden.

ISSN 1651-6214
ISBN 978-91-554-7944-2
urn:nbn:se:uu:diva-133112 (http://urn.kb.se/resolve?urn=urn:nbn:se:uu:diva-133112)

To the great ball of fusion fire that
provides light in the vast darkness

List of Papers

This thesis is based on the following publications, which will be referred to in the text by their Roman numerals.

I C. Platzer-Björkman, T. Törndahl, A. Hultqvist, J. Kessler and M. Edoff, Optimization of ALD-(Zn,Mg)O buffer layers and (Zn,Mg)O/Cu(In,Ga)Se_2 interfaces for thin film solar cells, *Thin Solid Films*, 515 (2007) p. 6024-6027.

II A. Hultqvist, C. Platzer-Björkman, T. Törndahl, M. Ruth and M. Edoff, Optimization of i-ZnO window layers for Cu(In,Ga)Se_2 solar cells with ALD buffers*, Proceedings of the 22nd European Photovoltaic Solar Energy Conference, Milano*, (2007) p. 2381-2384.

III A. Hultqvist, C. Platzer-Björkman, J. Pettersson, T. Törndahl and M. Edoff, $CuGaSe_2$ Solar Cells Using Atomic Layer Deposited Zn(O,S) and (Zn,Mg)O buffer layers, *Thin Solid Films*, 517 (2009) 2305-2308.

IV T. Törndahl, E. Coronel, A. Hultqvist, C. Platzer-Björkman, K. Leifer, and M. Edoff, The effect of $Zn_{1-x}Mg_xO$ buffer layer deposition temperature on Cu(In,Ga)Se_2 solar cells: A study of the buffer/absorber interface, *Progress in Photovoltaics: Research and Applications*, 17 (2009) p. 115-125.

V H. Marko, A. Hultqvist, C. Platzer-Björkman, S. Noël and J. Kessler, Effects of $CuIn_{0.5}Ga_{0.5}Se_2$ growth by isothermal and bithermal Cu-Poor/Rich/Poor sequence on solar cells, *Material Research Society Symposium Proceedings, Spring meeting*, San Francisco, 1165 (2009) M02-05.

VI J. Pettersson, C. Platzer-Björkman, A. Hultqvist, U. Zimmermann and M. Edoff, Measurements of photo-induced changes in the conduction properties of ALD-$Zn_{1-x}Mg_xO$ thin films, *Physcia Scripta*, Accepted.

VII T. Törndahl, A. Hultqvist, C. Platzer-Björkman and M. Edoff, Growth and characterization of ZnO-based buffer layers for CIGS solar cells, *Proceedings of the SPIE - The International Society for Optical Engineering*, San Francisco, 7603 (2010) p. 76030D-1-9.

VIII A. Hultqvist, C. Platzer-Björkman, E. Coronel and M. Edoff, Experimental investigation of $Cu(In_{1-x}Ga_x)Se_2/Zn(O_{1-z},S_z)$ solar cell performance, *Solar Energy Materials and Solar Cells*, Accepted, DOI: 10.1016/j.solmat.2010.09.009.

IX A. Hultqvist, M. Edoff and T. Törndahl, Evaluation of Zn-Sn-O buffer layers for $CuIn_{0.5}Ga_{0.5}Se_2$ solar cells, *Progress in Photovoltaics: Research and Applications*, Accepted, DOI: 10.1002/pip.1039.

X A. Hultqvist, C. Platzer-Björkman, U. Zimmermann, M. Edoff and T. Törndahl, Growth kinetics, properties, performance and stability of ALD Zn-Sn-O buffer layers for $Cu(In,Ga)Se_2$ solar cells, Manuscript

Reprints were made with permission from the respective publishers.

Personal contributions to the papers

I The article was written by Charlotte Platzer-Björkman. I did part of the solar cell fabrication and JV and QE measurements.

II I wrote the article, helped to develop the idea and did most of the solar cell fabrication and all of the measurements except for XRD.

III I wrote the article, helped to develop the idea and did all of the experimental work apart from the JVT measurements and analysis.

IV The article was written by Tobias Törndahl. I provided input on the measured results, did part of the solar cell fabrication, most of the JV and QE measurements and all of the optical measurements to determine the band gap.

V Hakim Marko wrote the article and I did part of the solar cell fabrication, all of the JV and QE measurements and took part in the project design and planning.

VI Jonas Pettersson wrote the article and developed the idea. I did the optical measurements to determine the band gap and discussed the results.

VII The article was written by Tobias Törndahl. I did part of the solar cell synthesis, most of the JV and QE measurements, some of the resistivity measurements and provided input on the result and discussion.

VIII I wrote the article, developed the project and did all of the measurements and analysis, except for XPS, XRD and STEM EDS.

IX I wrote the parts of the article that were not related to ALD development and took part in developing the project. I did most of the solar cell fabrication, the optical measurement, XRF, XRR, JV and QE.

X I wrote the article and developed the project. I did most of the solar cell and film fabrication and most of the XRR, XRF, JV, QE, resistivity and transmittance measurements.

Additional paper

C. Platzer-Björkman, A. Hultqvist, J. Pettersson and T. Törndahl, Band gap engineering of ZnO for high efficiency CIGS based solar cells, *Proceedings of the SPIE - The International Society for Optical Engineering, San Francisco*, 7603 (2010) p.76030F-1-9.

Contents

1. Introduction

The interest for energy production and sustainability of the Earths environment has recently escalated because of the currently strong dependence on the limited fossil fuels and because of the Earths environmental changes that have followed in the wake of human actions. A lot of effort is used to find good power sources that have a seemingly endless supply of energy and which do not affect the sustainability of the environment in the long run. The collective name for these types of power sources is renewable energies and they are generally divided into wave, hydro, tidal, wind and solar power. A common denominator for all of the categories is that their energy is provided by the sun either directly as for solar power or indirectly as for the others. The sun itself generates massive amounts of power, 10^{26} W [1], and although only a small part of that power, approximately1000 W/m^2 [2], reaches the Earth's surface, it is still enough to provide the current human demand several times [3]. Thus, harvesting power directly from the sun has a huge potential and has therefore received a lot of attention recently.

Solar power arrives as photons or light particles at the Earths surface and are normally absorbed or reflected by the surface. Absorbing the light generates heat in the absorbing material and was until the 19th century the only way of converting incident solar light into power. In 1839 however, Becquerel discovered that incident light on his electrolyte generated electricity [2], this effect was named photovoltaic from the Greek word phos meaning light and from voltaic meaning electric, originally named after the physicist Volta. As time passed and further research was performed, the effect was discovered in crystalline selenium [2] later also in silicon and was made into a power harvesting device called a solar cell that showed a promising conversion efficiency of 6 % in 1954 [4]. Currently, solar cells are being mass-produced to generate renewable energy and have an efficiency of up to 40 % on a lab scale and up to 20 % commercially [5]. As the solar cell market and installed power grows with 40 % per year [6] the competition to reduce the solar cell cost per Watt has become fierce.

One way of competing is to reduce the material costs by using less material in the solar cell. Typically the classical silicon solar cell technology uses a wafer with a thickness of a few hundred micrometers to convert the light. Another approach that only requires a hundredth of the Si wafer thickness and thus a lot less material is to use thin film technology to build the solar cell structure. While the thin film solar cells still do not achieve the same

performance as their silicon wafer counterparts [5] the reduced material usage makes them comparable in cost per Watt. An example of this is the thin film company First Solar which currently is one of the biggest solar cell companies to date and has the lowest official production cost per Watt of any large scale company.

While First Solar uses the CdTe compound for light absorption in their solar cells there are several other material options. Currently solar cells with amorphous silicon, CdTe or $Cu(In,Ga)Se_2$, CIGS, as the absorbing layer are competing with each other on an industrial scale, while less known materials as $Cu_2(Zn,Sn)(S,Se)_4$, CZTS, still are on a research stage. CIGS has shown the best conversion efficiencies of up to 20.3 % on a lab scale and up to 14 % [5] on an industrial scale and has therefore an advantage over the other materials as the race goes on towards lower costs per Watt.

Currently the standard technique of mass-producing CIGS solar cells and the technique of choice to achieve good conversion efficiencies include a CdS layer. Since cadmium is classified as a toxic material with restricted use in electronics [7] there are inherent problems of treating waste from the production and convincing customers that it is properly sealed inside without hazardous leaks. Extensive research, including this thesis, has therefore been performed to replace this layer with something that is nontoxic and that does not lower the performance [8-10]. As it turns out this is not as easy as it first seems, since the CdS layer has several beneficial properties for CIGS solar cells that are hard to reproduce with other materials. This thesis discusses these properties and other consequences of replacing the CdS layer with the alternative materials Zn(O,S), (Zn,Mg)O and Zn-Sn-O.

2. Basic concepts of CIGS Solar cells

2.1 Energy bands in a semiconductor

A solar cell is a device that transforms power from light directly into electricity. The first solar cell that showed interesting conversion efficiency of 6 % was fabricated in 1954 and was the result of the breakthrough in semiconductor technology during the late nineteen forties [4]. A semiconductor typically has a periodic structure of atoms, a crystal [2, 11]. The crystal arrangement limits the possible energies that the electrons of those atoms can have [2, 11]. At 0 K the total energy of all the electrons within the crystal is minimized and the highest energy electron state that is occupied by electrons is generally a band of electron states defined as the valence band maximum, E_v. The band is formed by overlapping electron states of atoms within the crystal. Similarly, there is an overlap of the lowest allowed unoccupied energy level or electron state of the atoms within the crystal that form a band of electron states defined as the conduction band minimum, E_c. In a semiconductor there is an energy gap or an interval of energies that are forbidden to be occupied by electrons in between the two energy bands defined as the band gap, E_g. At 0 K the valence band is completely filled with electrons so there are no free states for the electrons to move to unless they gain enough energy to cross the band gap and occupy states in the conduction band. It is thus impossible to transport small amounts of energy or electricity in the material and it acts as an insulator. As additional energy is provided to the crystal, the electrons have the possibility to absorb enough energy and occupy the conduction band. An electron in the conduction band, has an abundance of free states within a small energy interval and can therefore absorb and respond to energies that are a lot smaller than the band gap, thus acting quite differently than the electrons in the filled valence band. As electrons occupy the conduction band instead of the valence band they leave empty states behind, called holes, in the valence band. To occupy one of the empty states or holes in the valence band requires only a small amount of energy for an electron in the valence band and it is therefore possible to transfer energy even through the valence band if it is not completely occupied by electrons. A convenient way of treating holes is to define them as positively charged electrons that use a reversed energy scale in the band diagram. Once an electron occupies a conduction band state it also has a certain probability to loose part of its energy to crystal vibrations, other electrons or to light

emission. Since its new energy is too small to keep on occupying a state in the conduction band it transfers to an empty state with lower energy, possibly the valence band. The transfer process is generally denoted as recombination of a free electron and an empty state or hole. Applying an electric field to a semiconductor with electrons in the conduction band will give the electrons in the conduction band enough energy to move against the field and create a current, similarly the holes in the valence band will move along the field and also contribute to the current, thus the material is no longer the insulator it was when the conduction band was unoccupied but a conductor, hence the name semiconductor [2, 11].

By introducing impurity atoms that give rise to additional states within the band gap, acceptors, with unoccupied energy levels just above the valence band it is possible to have a material with an excess of holes at room temperature called a p-type material, since the energy at room temperature is enough for the electrons in the valence band to occupy the empty acceptor states [2, 11]. Similarly it is possible to generate a material with an excess of electrons in the conduction band, called n-type material, by introducing impurity atoms with states within the band gap or donors. If the donor state is introduced just below the conduction band the thermal energy provided at room temperature is enough for the donor state electron to occupy the conduction band [2, 11].

To predict if a specific energy level is occupied by an electron at a certain temperature the Fermi-Dirac distribution function, defined according to equation 2.1 [2,11], is readily used. Besides the Boltzmann constant k there is another constant in equation 2.1 denoted E_F, or the Fermi energy, for which the Fermi-Dirac distribution function value is exactly one half.

$$f_{FD} = \frac{1}{1 + e^{\frac{E - E_F}{kT}}} \qquad (2.1)$$

In a semiconductor without any donors or acceptors the E_F is situated in the middle of the band gap since the probability of finding a free electron in the conduction band is exactly the same as finding a hole in the valence band. On the other hand if donors are introduced close in energy to E_c, E_F will shift towards E_c because the probability of finding a free electron in E_c at a moderate temperature is larger due to the donors than finding a hole in E_v. Similarly a downwards shift of E_F occurs if acceptors are introduced.

2.2 The ideal p-n junction

The solar cell is a special type of diode and it is therefore useful to understand how a diode works. A diode consists of an n-type material that is adjacent to a p-type material, as shown in figure 2.1.

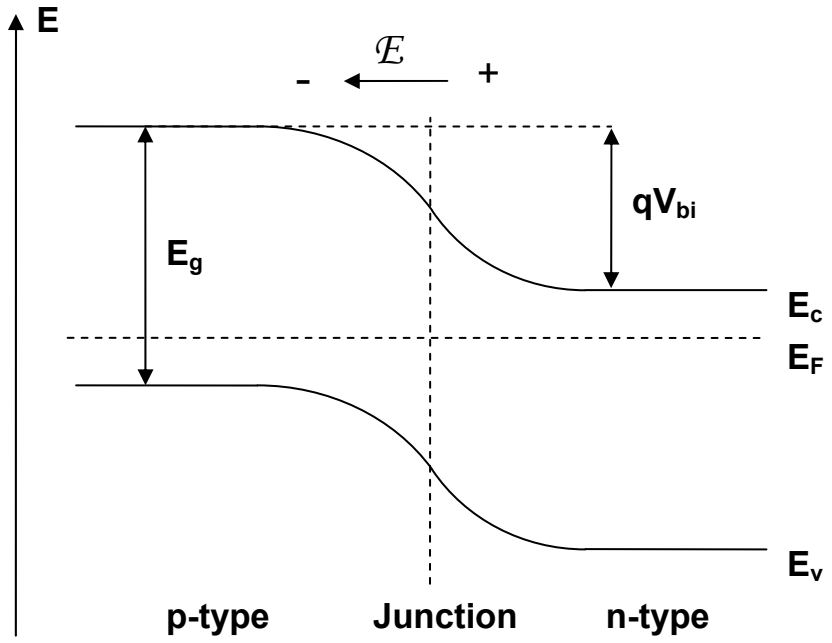

Figure 2.1. The ideal p-n homojunction at equilibrium.

Since there is an excess of conduction band electrons in the n-type material they will diffuse towards the p-type material and similarly since there is an excess of holes in the p-type material they will diffuse towards the n-type material. As the electrons and holes diffuse they alter the charge distribution of the materials since the ionized donors and acceptors remain fixed within the crystal lattice. This creates an electric field across the material junction that counteracts the diffusion so that the net flow of electrons and holes is zero between the two materials at equilibrium. The electric field extends in a region surrounding the junction denoted as the space charge region, SCR, and the resulting potential after integrating the field in this region is called the built in potential, V_{bi} [2, 11]. V_{bi} is an indirect measure of the energy band bending that is a required to keep E_F constant throughout the junction at equilibrium. As a result of the band bending the conduction band occupies a lower energy in the n-type material compared to in the p-type material. It is therefore easier for an electron to travel from the p-type material to the n-type material since it does not need to absorb additional energy to overcome the electric field as it would have to if it went from n-type to p-type and it is similarly easier for a hole to travel from n-type to p-type than from p-type to n-type. This barrier in the energy bands, can be manipulated by applying a potential from the p-type to the n-type material. As the potential is lowered the barrier increases and the SCR widens. It is not very likely that the electrons in the conduction band of the n-type material will be able to cross the

increased barrier. There is however a small negative current since a small amount of free electrons will be in the conduction band of the p-type material at room temperature and some of those will be pulled by the electric field towards the n-type material. However, as forward bias is applied the barrier is reduced and at some point it is low enough to enable a significant diffusion of conduction band electrons from n-type into p-type and similarly of holes from p-type to n-type leading to a large forward current. The resulting current density-voltage, JV, relationships is shown in figure 2.2 and is generally analytically expressed as equation 2.2 [2, 11], where k is the Boltzmann constant, J_0 the saturation or dark current, T the crystal temperature and q the electron charge.

$$J = J_0(e^{\frac{qV}{kT}} - 1) \qquad (2.2)$$

2.3 The solar cell

Compared to other diodes the solar cell is able to efficiently convert incoming light into electrical power and deliver it to a load. Light comes in small wave packages defined as photons, which carry energy [2, 11]. Through the photovoltaic effect the photon energy can be absorbed by an electron. If the electron were to be in the valence band at the time and received enough energy it could be excited to a level in the conduction band. In a diode this leads to three possible cases. In the first case the electron is excited into the conduction band of the depletion region which means that it will be separated from its hole because of the electric field and as a result a small current would arise. For the other two cases in which the electron is excited in either the bulk p-type or n-type material, a charge separation has a probability to occur if the electron or its corresponding hole diffuses into the depletion region. Thus as long as there is a depletion region, excited electrons will be separated from their holes almost independently of the bias across the junction and the incoming light can therefore be simplified as a constant light current density offset, J_L, to the diode equation as shown in equation 2.3 [2, 11].

$$J = J_0(e^{\frac{qV}{kT}} - 1) - J_L \qquad (2.3)$$

An example of the difference in JV characteristics for a solar cell diode in darkness and with incident light is found in figure 2.2.

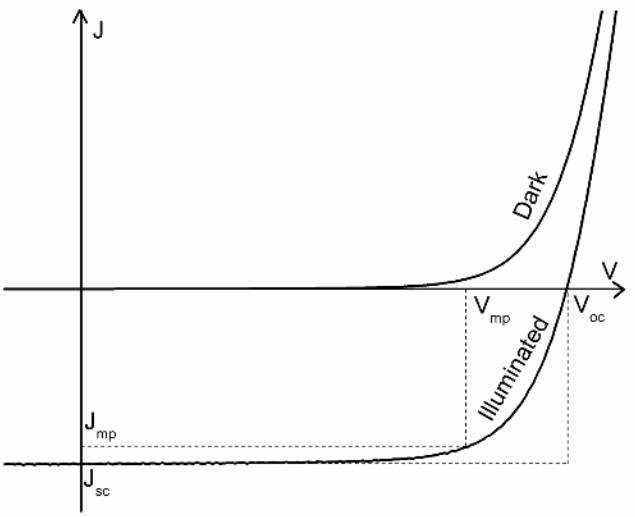

Figure 2.2. JV characteristics of a solar cell

The current that passes through the solar cell when no bias is applied across it is defined as the short circuit current and is regularly normalized with respect to the solar cell area as a current density, J_{sc}. The value of J_{sc} is determined by how many of the incoming photons that are converted into excited electrons and how many of those that reaches the contacts. The voltage where the forward bias diffusion current equals the light induced current is defined as the open circuit voltage V_{oc}. This parameter is dependent on V_{bi} or indirectly E_g, temperature and the dark reverse bias current J_0, which in turn is dependent on the material properties of the p-n junction and on non ideal leakage currents across the junction. Finally the fill factor, FF, is a measure of how close to $V_{oc} \cdot J_{sc}$ that the solar cell can operate at in its maximum power point, the point where the product of V·J reaches it maximum and is calculated according to equation 2.4 [2, 11].

$$FF = \frac{V_{mp} \cdot J_{mp}}{V_{oc} \cdot J_{sc}} \qquad (2.4)$$

The FF is affected by the total series resistance, R_s, across the solar cell and by shunt conductance, G_{sh}, due to electrical paths that circumvent the p-n junction, including these effects into the diode equation results in equation 2.5 [12].

$$J = J_0 (e^{\frac{q(V - JR_s)}{kT}} - 1) + G_{sh}(V - JR_s) - J_L \qquad (2.5)$$

If the incident power is known it is easy to calculate the conversion efficiency of the device according to equation 2.6 [2, 11] as the maximum power of the device divided by the incoming light power.

$$\eta = \frac{V_{oc} \cdot J_{sc} \cdot FF}{P_{in}} \qquad (2.6)$$

Absorption of light across the band gap is affected by the crystal structure not only due to the size of the band gap, but also due to how those bands relate to the momentum of the crystal. In the simplest case an electron that absorbs a photon energy that is large enough to transfer it from the highest occupied valence band state to the lowest unoccupied conduction band state only requires energy, this case is called a direct band gap [2, 11]. However, in some materials such a transition is not allowed since it would require a transfer of momentum as well. Since the photons have negligible momentum a second interaction with the lattice or other electrons needs to take place to give the excited electron enough momentum to occupy a state in the lowest unoccupied conduction band state. Materials with these requirements have reduced light absorption properties due to this and are defined to have indirect band gaps [2, 11]. Silicon is an example of a material with an indirect band gap and this is part of the reason why the silicon solar cell technology is based on relatively thick wafers of around 100-200 μm [2, 11].

Additionally, it is important to choose a band gap size that matches the spectrum of the sunlight at Earths surface shown in figure 2.3 [2, 11].

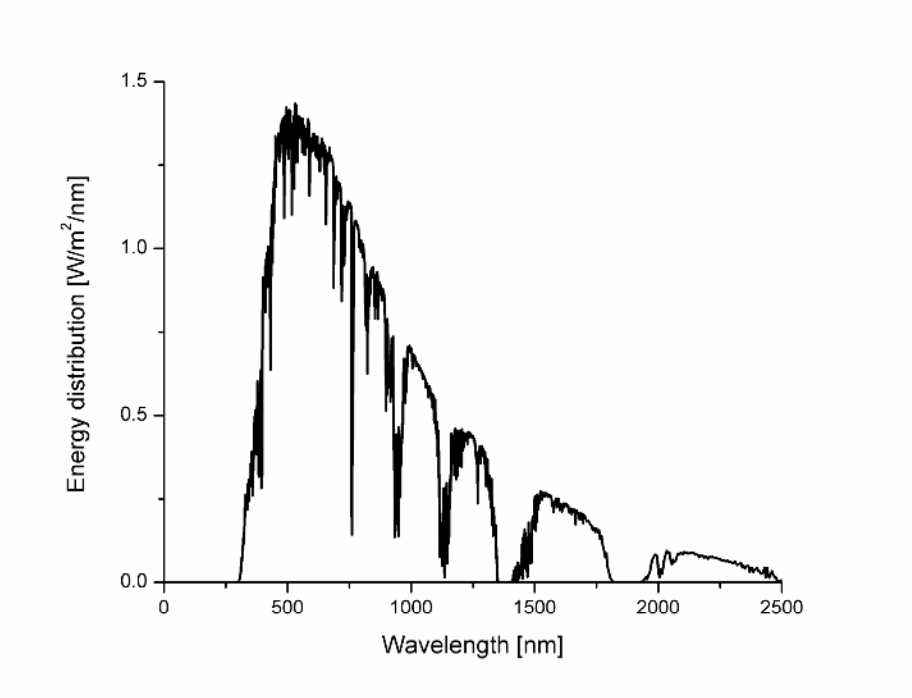

Figure 2.3. Spectral distribution of sunlight

The photon energy, E, is related to the wavelength, λ, of the light through equation 2.7 [2, 11] where h is the Plank constant, c is the speed of light.

$$E = \frac{hc}{\lambda} \qquad (2.7)$$

Thus by choosing a material with a small band gap more photons would be absorbed by the material and thus increasing J_{sc}. However, a small band gap would also mean that the V_{oc} of the device would drop since the required voltage to generate the large forward diffusion current across the p-n junction is decreased for smaller V_{bi} or indirectly E_g. Taking both aspects into account an optimum is found for a band gap of around 1.4 eV for the incoming sun light spectrum [2]. Good conversion efficiencies can still be achieved in the 1.0 to 1.7 eV range as for silicon solar cells which have a 1.1 eV band gap.

A solar cell material with a slightly larger band gap than crystalline Si or a direct band gap would have an advantage over the crystalline silicon solar cell technology in terms of theoretical efficiency and material usage respectively. There are several candidate materials that in theory have both or one of these advantages as amorphous Si, GaAs, CdTe, $Cu(In,Ga)Se_2$, GaN, and $Cu_2(Zn,Sn)S_4$. While GaAs has shown the highest performing solar cells to date it requires fairly slow and energy consuming deposition processes for good devices. Research on $Cu_2(Zn,Sn)S_4$ and GaN has just started and the

materials are not ready for industrialization. Which leaves amorphous Si, CdTe and $Cu(In,Ga)Se_2$, where $Cu(In,Ga)Se_2$ so far is in the lead on a lab scale and has therefore received a lot of research attention including the work in this thesis [8-10, 13-15]. The problem with $Cu(In,Ga)Se_2$ and CdTe is that they cannot be made both n and p type in a controlled manner to form a p-n junction of the same material or a homo junction, but need another material to form the junction, a junction of this type is defined as a hetero junction [2, 11].

2.4 Non ideal p-n junction

A hetero p-n junction differs from the previously discussed junction in the sense that the two materials have different band gaps and electron affinities. The electron affinity, χ, is a measure of the required energy to excite an electron from the conduction band to the vacuum level. In the ideal case, called the Anderson model, perfect crystals exist on both sides all the way to the junction [2, 11]. Assuming this, it is possible to form the p-n junction by keeping the vacuum level continuous across the junction as is shown in figure 2.4. Due to the dissimilarities in band gap and electron affinity, a discontinuity, calculated according to equation 2.8 [11], is formed in the conduction band defined as the conduction band offset, CBO, and another calculated according to equation 2.9 [11], in the valence band defined as the valence band offset, VBO.

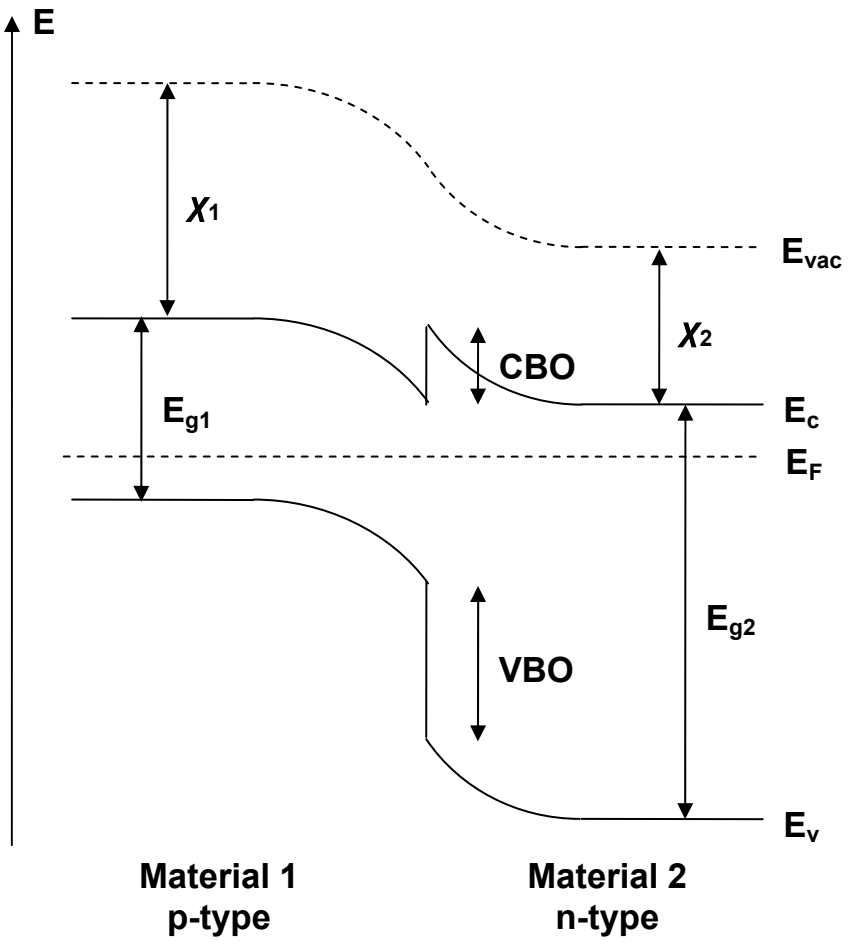

Figure 2.4. The ideal p-n hetero junction

$$CBO = q(\chi_2 - \chi_1) \qquad (2.8)$$

$$VBO = E_{g1} + q\chi_1 - E_{g2} - q\chi_2 \qquad (2.9)$$

In reality the two materials reconstructs close to the interface to minimize the total crystal energy, which changes the crystal properties at the interface [16-18]. It is also of importance how the crystals are aligned toward the interface since different surface planes of the crystals have different properties both electrically and structurally [18]. In general there is also a difference in the crystal lattice constant between the two materials which introduces dangling bonds or unoccupied states at the interface since the crystals do not match each other perfectly [2, 17]. All these effects change the charge distribution away from the ideal case and therefore also affect the depletion region width and the band bending of the conduction and valence bands [2, 17]. Additionally, the extra states at the interface or in the interface recon-

struction layer could be situated within the band gap of the two materials providing possible pathways for leakage currents through the junction [2, 17].

Things are no different for CIGS solar cells where CIGS normally is p-type as grown due to its internal imperfections in the crystal, but cannot become n-type in a controlled manner and a second quite different n-type material, normally CdS, is therefore used to complete the junction [15]. However, since cadmium is classified as toxic and since the band gap of CdS is small enough to absorb some of the incoming high energy photons without collecting them it is of great interest to replace this layer by another n-type semiconductor that is transparent to sunlight. Unfortunately, the material properties of CdS and the way that it forms the p-n junction with the CIGS seems to be very crucial for good solar cell performance and have so far been hard to reproduce with other materials. Several studies both theoretical and empirical including this thesis have therefore addressed either of the questions why the CdS works so well or why other materials have a hard time achieving the same solar cell performance [8-10, 19-22]. To further complicate the hetero junction picture, CIGS and CdS or its replacement are almost exclusively polycrystalline materials, thus introducing even more uncertainties at the interface regarding what happens at grain boundaries of different types, what effect the variations between the grains have on the overall performance and how the properties of the subsequent material are affected by the underlying surface during growth [12, 23].

In short solar cells can straightforwardly be explained by simple diode equations, but in reality as will be shown in this thesis for CIGS solar cells there are plenty of deviations from the ideal behavior of equation 2.5.

3. The $Cu(In,Ga)Se_2$ solar cell stack

3.1 Synthesis of the $Cu(In,Ga)Se_2$ solar cell stack

In the previous chapter solar cells were described to have one or two materials that formed a p-n junction. In practice the typical CIGS solar cell [8, 15, 24] consists of five layers and a substrate as illustrated in figure 3.1.

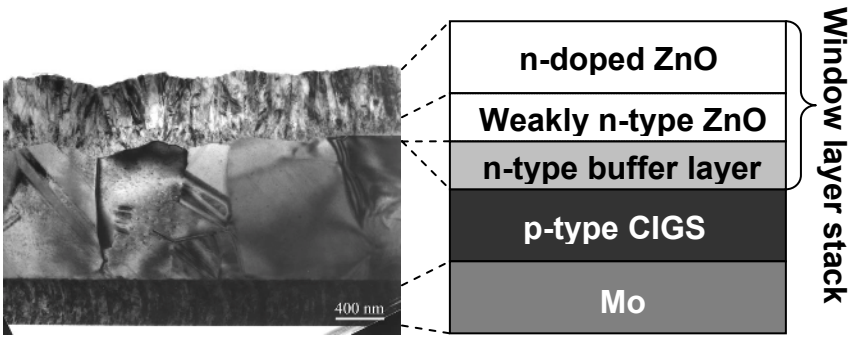

Figure 3.1. A micrograph and a schematic of the CIGS solar cell thin film stack.

Starting from the bottom the substrate consists of one or several mm of either glass or other more flexible materials as steel or different types of plastic. The substrate gives support and rigidity to the thin solar cell layers and in the case of soda lime glass it provides a supply of Na atoms that is proven to be beneficial for growth and device performance [15]. In this study the glass substrates are cleaned following a baseline process to remove any dirt on the surface prior to the subsequent depositions [25].

A thin layer of polycrystalline Mo normally 300-400 nm [8, 15, 24] is deposited by sputtering on the substrate and acts as the low resistance, ohmic, back contact to the p-type CIGS. Even though the reflectivity of the Mo film is not great it does reflect some of the light that was not absorbed by the CIGS back into the material for an additional pass, which further increases the probability that the light is absorbed in the solar cell. The Mo films in this study are deposited with DC sputtering according to a baseline process [24]

Polycrystalline p-type CIGS is co-evaporated on the Mo layer to a thickness of 1 to 2 μm. The CIGS thin film is sometimes called the absorber layer since it is designated to absorb the incoming sunlight. By changing the

amount of Ga to In normally defined according to equation 3.1, it is possible to change the CIGS band gap from 1.0 eV at x = 0 to 1.7 eV at x = 1 while maintaining a direct band gap [25].

$$x = \frac{[Ga]}{[Ga]+[In]} \qquad (3.1)$$

As discussed in the previous chapter the ideal band gap would be somewhere around 1.4 eV for a solar cell which would imply that x = 0.6 for the CIGS film. In reality the best devices are found close to x = 0.3 or a band gap of 1.1 eV [15], due to lower than expected V_{oc} and FF for higher x-values [26]. However, since it is possible to vary the band gap by the Ga content it is also possible to grow a graded band gap or a depth profile in the x-value and possibly increase the solar cell performance. One way to utilize this is to increase the band gap at the top and bottom interfaces of the CIGS layer to possibly lower the dominant recombination current and thereby increase V_{oc}, while maintaining a low band gap in the middle to keep a good absorption and collection [27]. As of today some of the best CIGS solar cells ever made have graded band gap depth profiles [28]. The quality of the CIGS solar cells is also dependent on the Cu content, y, of the film, which is defined according to equation 3.2.

$$y = \frac{[Cu]}{[Ga]+[In]} \qquad (3.2)$$

Solar cells with y-values in the range of 0.6-1.0 are able to retain both the CIGS lattice and the performance [25]. As the y-value is increased above 1.0 conductive Cu_xSe starts to segregate from the film, which severely degrades the performance of the solar cell by decreasing the FF through an increased shunt conductance [29]. However, having a y-value above 1.0 also improves the grain quality. This positive effect can be utilized through having a Cu rich part of the CIGS deposition to improve the grain growth and lower the Cu rate later towards the end of the deposition so that the final film ends up without any Cu_xSe and with a y-value of less than 1.0. Compared to constantly having a y-value below 1.0 or above 1.0 the solar cell performance of those with a Cu rich stage that ends Cu poor have an improved performance. This technique is for example used in the latest CIGS world record cells [29, 30]. In this study similar co-evaporation schemes, listed in table 3.1, are used for the growth of CIGS.

Table 3.1. *The CIGS schemes used for the different studies in this thesis*

CIGS scheme	Used in paper	Reference
CUPRO	III, IV, V, VII, VIII and IX	[31]
Cu poor, Cu rich inline	I, III and VII	[24]
Inline	I, II, IV, VII and X	[32]

As discussed earlier an n-type layer is required to complete the p-n junction with CIGS. Historically this layer consisted of only one material, but later evolved into three separate layers [8, 15, 24] with the collective name window layer stack. The reason why it is denoted window is that all of the materials in the stack are transparent or almost transparent to sunlight, since it is preferable to absorb all light in the CIGS [8, 9].

The top of the window layer stack consists of a transparent conductive layer that acts as the contact to the n-type layer. In this study that layer is deposited with radio frequency, RF, magnetron sputtering to a thickness of 200-300 nm and it consists of ZnO heavily doped with aluminum, ZnO:Al, to enhance the conductivity. A problem of transparent conductive films is that they generally require high levels of doping or a large amount of free electrons or holes at room temperature to increase the conductance. The free electrons are able to screen the incoming light and thus reflect it if it is above a certain wavelength according to Drude theory [17]. This wavelength is moved towards shorter wavelengths if the concentration of free carriers is increased in the material and can therefore reduce the transmittance of the material especially for longer wavelengths. Additionally, small amounts of energy can easily be absorbed by the free electrons reducing the low energy or long wavelength light transmission even further. There is thus a tradeoff between a high conductivity and good transmittance of the material.

Below the top contact an intermediate 50-100 nm thick layer with unintentionally n-type doped ZnO, i-ZnO, is deposited by RF magnetron sputtering [8, 15, 24]. While this layer has a substantially lowered conductivity compared to the top layer and thus increases the device R_s as it thickens, a thin layer is beneficial for FF [33]. The basic idea behind the improved FF is that the i-ZnO layer prevents shunt current paths around the p-n junction. In the extreme case there might be a pinhole in the CIGS enabling a direct contact between the Mo back contact and the ZnO:Al, which vastly reduces FF [33]. Preventing shunts with an i-ZnO layer is especially useful as the area of the cell or module is increased, since the increased size makes it harder to grow CIGS without local non-uniformities. On the other hand if the CIGS layers could be deposited with a better uniformity or if the shunt preventing properties of the i-ZnO could be included in another layer, the i-ZnO layer would no longer be required.

Finally, at the bottom of the window layer stack, right on top of the CIGS layer a thin layer defined as the buffer layer is deposited. Its name derives from the function of acting as a stepping stone electrically and optically between the p-type CIGS and the n-type ZnO layers. This layer is critical since it defines the p-n junction quality and the device performance when it is deposited on the CIGS and has therefore received a lot of attention from researchers including this thesis [8-10]. The standard process is to grow 50-70 nm of CdS by chemical bath deposition, CBD, since it is the buffer layer that gives the best solar cell performance as of today [5]. As the name indi-

cates the substrate is submerged into a solution containing chemicals that reacts with each other and forms CdS on the CIGS surface during the CBD. This method is considered to be soft since the CdS atoms arrive at the surface with a low kinetic energy. On the other hand the solution contains ammonia that has shown to etch away surface contamination as organic carbon compounds and oxides. This etching effect is believed to be another reason behind the success of CdS [9]. Additionally, CBD gives conformal coatings even for rough surfaces such as those of the polycrystalline CIGS [8], which enables the formation of a good p-n junction over the entire surface. In order to replace the toxic CdS, alternative buffer layers need to mimic these properties or compensate for them by other means in order to perform as well as CdS. As an example, using sputtering, spraying or evaporation to deposit the alternative buffer layer straight onto CIGS has yet to show the same performance [8-10] as the CdS references. CBD of other materials as Zn(O,S) shows promising results but has a lot smaller process window and controllability compared to the CdS process [8-10]. The main method to deposit alternative buffer layers in this study that also shows excellent results, in some cases even better than the CdS references, is atomic layer deposition, ALD.

3.2 The CUPRO process

In the studies contained within this thesis the CIGS co-evaporation scheme denoted copper-poor/rich/then off, CUPRO, is frequently used and in one study modified. As the name indicates the Cu evaporation rate is varied in three stages during the CUPRO process, as seen in figure 3.2, while the evaporation rates of In, Ga and Se and the substrate temperature are kept constant.

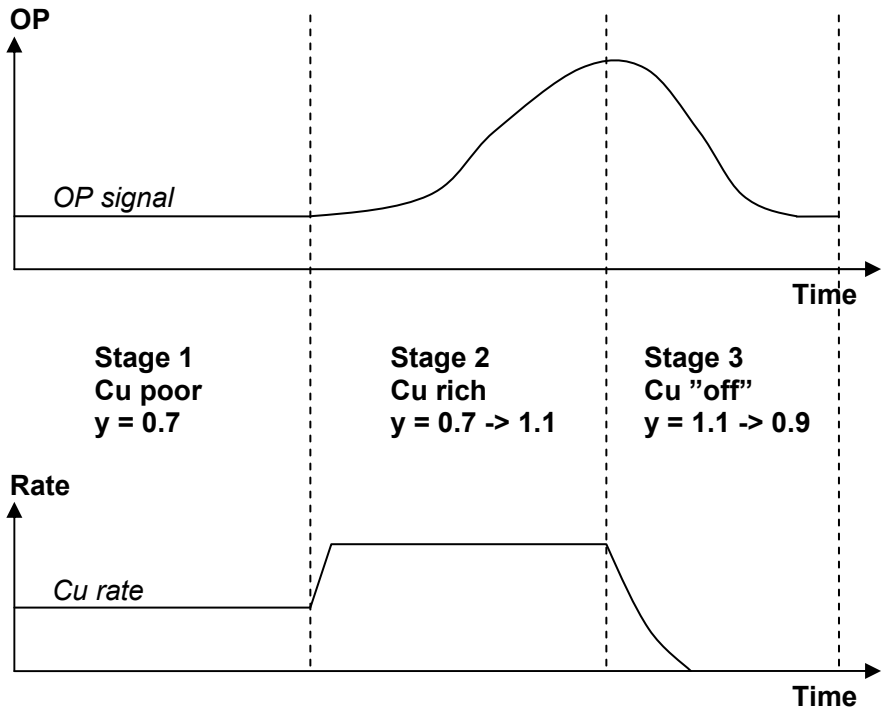

Figure 3.2. The CUPRO co-evaporation scheme showing the three deposition stages and the corresponding Cu rate and substrate OP signal.

The first stage of the CUPRO process starts by growing Cu poor CIGS, chosen in this study to have y = 0.7. To utilize the improved grain quality of growing at y>1 the Cu evaporation rate is increased at the start of the second stage, so that resulting CIGS has y>1. It is possible to monitor the transition from Cu poor to Cu rich CIGS by measuring the operating power, OP, needed to keep the substrate temperature constant. An increased OP is required to keep the substrate temperature constant when Cu_xSe segregates at the surface, as seen in figure 3.2, since the emissivity of Cu_xSe is higher than that of CIGS [29]. The Cu evaporation rate is kept high until the substrate OP signal no longer increases with time. At this point the third stage starts by turning off the power to the Cu source which rapidly diminishes the Cu evaporation rate. Even though the Cu rate is low or zero, CIGS keeps forming on the surface during this stage since the segregated Cu_xSe acts as a Cu source. As the Cu_xSe is used to form CIGS the substrate OP signal decreases due to the decreasing amount of high emissivity Cu_xSe. The OP signal finally saturates when all of the Cu_xSe is used up, resulting in CIGS with a y-value of approximately 0.9, this also marks the end of the CUPRO process. The ability to monitor the transitions in y-value by measuring the substrate OP makes it possible to determine when to terminate the deposition, which has granted these types of process schemes the notation “end point detec-

tion". In paper V the CUPRO process is modified by having a low substrate temperature during the first stage, increasing it at the start of the second stage and keeping it high for the remaining part of the deposition.

3.3 Atomic layer deposition

In our ALD process Zn, Mg and Sn are bonded to a metal organic ligand [34]. Volatile precursors are used to increase the vapor pressure of the element enough to be able to transport it in a gas phase. In this thesis diethyl zinc, $Zn(C_2H_5)_2$ or DEZ and H_2O are used as the precursors for Zn and O respectively to deposit ZnO [35]. In the F120 microchemistry and the home-built MP3 ALD reactors that are used within this thesis, the precursors are admitted into a carrier gas, in this case N_2. The carrier gas flows past the precursor source valves where it is diluted by the precursor and then into the heated chamber. As the gas reaches the heated substrate holder it is designed to flow in a uniform laminar manner over the surface of the substrate and then into an exhaust pipe that leads to a roughing pump. Additionally, since ALD transports the elements with a carrier gas it is possible to grow conformal films even on rough surfaces like CIGS [36]. Figure 3.3 illustrates the schematic ALD process for ZnO. The process starts in a) by introducing DEZ into the carrier gas. DEZ reacts with the -OH groups at the surface and forms C_2H_6 as ZnC_2H_5 is bonded to the oxygen atom of the film. This process continues until all of the films -OH groups have reacted or until it is no longer possible to chemisorb more ZnC_2H_5 to the surface. In b) the DEZ valve is closed and weakly bonded adsorbates desorb from the surface. H_2O is introduced into the carrier gas in c) and it reacts with the possibly remaining $-C_2H_5$ groups of the surface and forms C_2H_6 as an -OH group is bonded to the zinc atom. Similarly to b) this process continues until all $-C_2H_5$ groups have reacted and the surface is terminated by a coverage of -OH. The water is removed from the carrier gas in d) and anything that is weakly bonded to the surface desorbs during the N_2 purge pulse. Since the surface is now terminated by OH groups it is possible to restart from a) to increase the thickness of the film. The process flow from a) to d) is commonly denoted as an ALD cycle [34]. Within this thesis a $DEZ/N_2/H_2O/N_2$ notation is used to describe the ALD ZnO cycle.

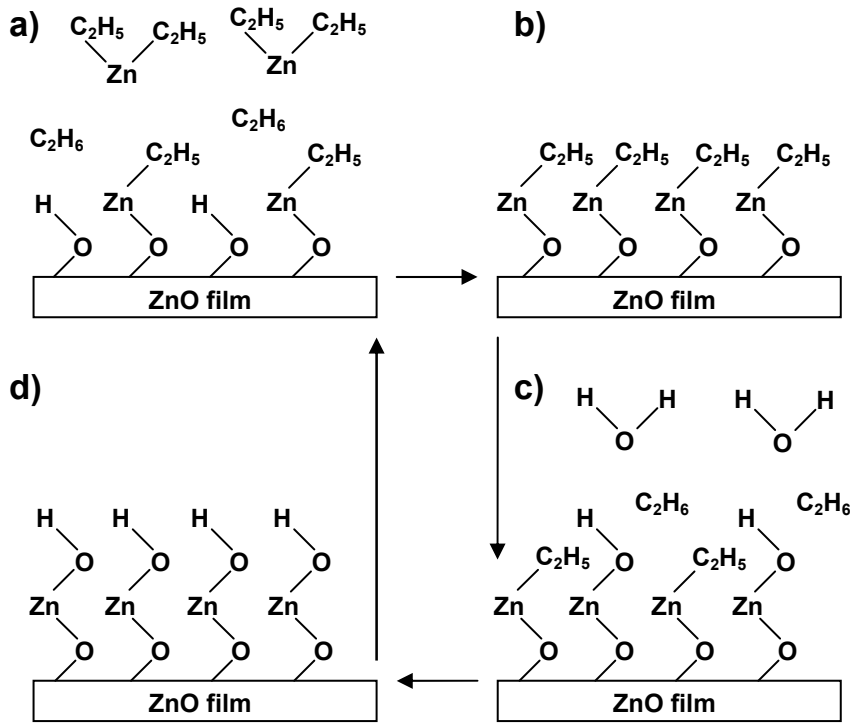

Figure 3.3. A schematic of the ALD cycle used to deposit ZnO. The four step pulse sequence starts in a) by introducing diethyl zinc, which reacts with the OH groups of the surface and forms C_2H_6. After the reaction has saturated anything that does not stick to the ethyl groups at the surface is purged away in b) with N_2. Water is introduced in c), which reacts with the ethyl groups of the surface and forms C_2H_6. Another N_2 purge is introduced after the second reaction is saturated in d) to remove reaction products from the surface of the film.

To form the ternary buffer layer compounds used in this thesis the ALD cycle for ZnO is modified. Zn(O,S) is grown by replacing some of the $DEZ/N_2/H_2O/N_2$ cycles by $DEZ/N_2/H_2S/N_2$ cycles, where H_2S is used as the S precursor. By controlling the ratio of H_2S cycles to H_2O cycles, the resulting S content z, defined according to equation 3.3, of the Zn(O,S) film can be controlled.

$$z = \frac{[S]}{[O]+[S]} \qquad (3.3)$$

There are however some control issues for the Zn(O,S) process, since there is constantly a $ZnO + H_2S \Leftrightarrow ZnS + H_2O$ reaction taking place as H_2O or H_2S are introduced into the chamber. Additionally, the Zn(O,S) films have a higher S content at the interface towards CIGS if they are deposited in solar cells. The reason for this is not known and could be the cause of multiple simultaneous processes. One possible reason could be that the incubation

time for growth on CIGS is longer for ZnO than for ZnS and another that H_2S more easily removes oxygen from the Zn(O,S) film at the nucleation stage when the bulk volume of the film is small.

The Mg precursor used for (Zn,Mg)O films is cyclopentadienyl magnesium, $Mg(C_5H_5)_2$ or $MgCp_2$. By controlling the ratio of DEZ/N_2/H_2O/N_2 cycles to $MgCp_2$/N_2/H_2O/N_2 cycles in the ALD process it is possible to control the Mg content w, defined according to equation 3.4, of the (Zn,Mg)O films in an excellent manner.

$$w = \frac{[Mg]}{[Zn]+[Mg]} \qquad (3.4)$$

To control the Sn content u, defined according to equation 3.5, of Zn-Sn-O films the ratio of DEZ/N_2/H_2O/N_2 cycles to Sn precursor/N_2/H_2O/N_2 cycles is changed in the ALD process. Tin(IV) t-butoxide, $Sn(C_4H_9O)_4$ is used as the Sn precursor in paper IX. Unfortunately, this precursor includes oxygen and since it is also a chemical vapor deposition precursor it is designed to crack at a certain temperature and grow SnO_x by itself. This makes it hard to control in ALD since its reaction with the surface does not self terminate, instead a linear growth rate is observed for increasing pulse lengths. The resulting films are uniform over the surface, but become more and more Sn rich as they get thicker, possibly because of nucleation problems for the $Sn(C_4H_9O)_4$ precursor on CIGS. Additionally, in paper IX it is shown that 8 consecutive cycles of Sn precursor/N_2/H_2O/N_2 are required to deposit SnO_x on ZnO or to include Sn into a Zn-Sn-O film, which significantly elongates the deposition time. In paper X a different ALD precursor tin(IV) dimethylamide, $Sn(N(CH_3)_2)_4$ is used to improve the growth control of Zn-Sn-O. This precursor creates uniform films both over the surface and with respect to thickness and does not require consecutive pulses to grow on ZnO.

$$u = \frac{[Sn]}{[Zn]+[Sn]} \qquad (3.5)$$

Table 3.2 lists which precursors and ALD reactors that has been used to grow the ALD buffer layers within this thesis.

Table 3.2. *List of the precursors and chambers used for the ALD of buffer layers within this thesis.*

Buffer layer	Precursors	ALD Reactor	Used in paper
Zn(O,S)	Zn: diethyl zinc, $Zn(C_2H_5)_2$ O: H_2O S: H_2S	F-120	III, VII and VIII
Zn(O,S)	Zn: diethyl zinc, $Zn(C_2H_5)_2$ O: H_2O S: H_2S	MP3	II, V and VIII
(Zn,Mg)O	Zn: diethyl zinc, $Zn(C_2H_5)_2$ O: H_2O Mg: cyclopentadienyl magnesium, $Mg(C_5H_5)_2$	F-120	I, II, III, IV, VI and VII
Zn-Sn-O	Zn: diethyl zinc, $Zn(C_2H_5)_2$ O: H_2O Sn: tin(IV) t-butoxide, $Sn(C_4H_9O)_4$	F-120	IX
Zn-Sn-O	Zn: diethyl zinc, $Zn(C_2H_5)_2$ O: H_2O Sn: tetrakis(dimethylamino) tin, $Sn(N(CH_3)_2)_4$	F-120	X

4. Analysis of $Cu(In,Ga)Se_2$ solar cells and material properties of individual layers

In order to compare the finished solar cells or thin films, several analysis methods are applied. Some of the key methods are explained in detail in this chapter, while the remaining methods are summarized as a table at the end of the chapter.

4.1 Current density versus voltage measurements

Measuring the JV curve is a way to quickly determine the overall performance of the solar cell. The JV setup consists of a light source, a shutter, a sample stage with a controlled temperature, a source measuring unit, SMU, and computers that control the measurement. A tungsten halogen lamp is used for the studies within this thesis as a light source. While the lamp is able to provide 1000 W/m^2 it has a different spectral distribution compared to sunlight. The light intensity of the lamp is calibrated by adjusting its distance from the sample stage so that a reference Si photodiode (Hamamatsu S1337-66BR) or a certified CIGS reference solar cell generates the same J_{sc} as it does in sunlight. Since there is a big dissimilarity in band gap between CGS and the two calibration samples a CGS reference cell with a J_{sc} measured by quantum efficiency, QE, is used to adjust the distance between the lamp and the stage in paper III. A computer keeps the sample stage temperature at 25 °C by reading the temperature with a thermo coupler and adjusting the temperature with water cooled Peltier element. An SMU is used to sweep the bias across the solar cell while simultaneously measuring the current. The resulting JV curve data is sent to a computer where it is saved and plotted, in a similar manner to figure 2.2. Additionally, the computer program automatically determines V_{oc}, J_{sc}, FF and η for the measured solar cell. A JV curve can also directly provide information about losses in FF. A high R_s decreases the exponential part of the current density according to equation 2.5 whereas a high G_{sh} increases the influence of the shunt current density. Furthermore, a JV curve can easily illustrate other non ideal characteristics as kinks or double diodes. The light exposure time is controlled by a shutter that is placed in between the solar cells and the lamp. Normally the shutter is only open during the JV sweep to avoid additional effects of extended light

exposure. However, during light soaking post treatment the shutter is kept open, which exposes the solar cells to light for an extended period of time.

4.2 Quantum efficiency

To get a better understanding of the light collection dynamics that generate the photocurrent external quantum efficiency, QE, measurement can be performed on the completed solar cells. The external QE for a certain wavelength is defined as the percentage of the incoming photons that are absorbed by the solar cell and converted into electrical current. Two examples of this measurement are shown in figure 4.1. In order to perform a QE measurement it is therefore important to both be able to generate and select monochromatic light or light of a specific wavelength in a controlled manner. This is realized using a xenon short arc lamp and by letting the generated light pass through a monochromator and a filter wheel. In order to estimate the monochromatic light intensity from the lamp, part of the light is directed towards a reference cell which absorbs the light and generates a current, while the rest of the light is fed through an optical fiber to the sample stage. To find out what the intensity is at the sample stage another reference cell is placed there which generates a current. A lock-in amplifier measures the two currents and sends the values to a computer which calculates the relation between the two currents, making it possible to know the intensity at the sample stage by only measuring the lamp intensity during a regular measurement. The measurement light of the setup is also chopped at a frequency of 77 Hz so that the lock-in amplifier can distinguish it from possible background light sources. By letting the computer control the filter wheel and the monochromator it is possible to sweep the wavelength of the measurement light and measure the QE for a test solar cell at each wavelength. Typically the wavelength interval is chosen to coincide with that of sunlight, since by knowing the QE at each wavelength and the spectral distribution of sunlight it is possible to calculate a theoretical current density value for a specific voltage across the solar cell. Due to limitations of the setup the solar cells in this study are measured at short circuit conditions, which automatically gives J_{sc} and without any light bias. Adding an uncalibrated light bias does not change the QE of the solar cells in this study, except for some of the CGS solar cells using (Zn,Mg)O buffer layers found in paper III where the QE drops slightly.

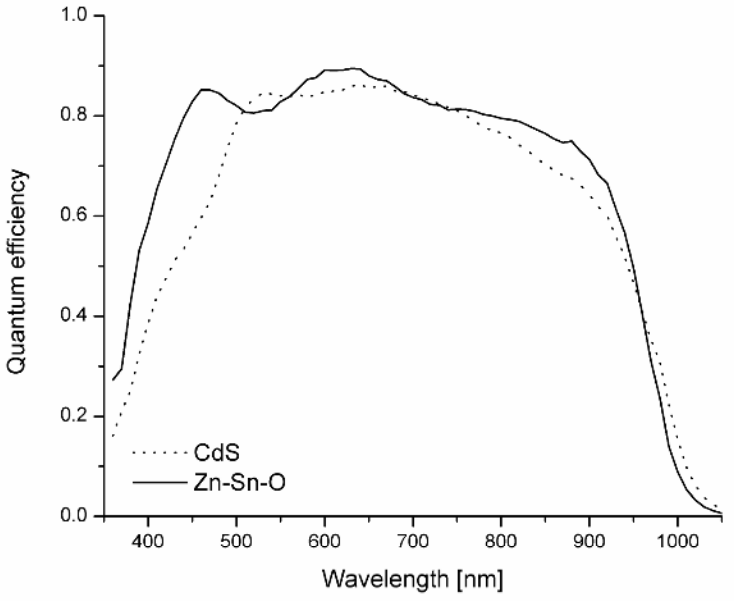

Figure 4.1. Quantum efficiency for two CIGS solar cells with different buffer layers.

There are a few wavelength regions of interest in a QE measurement that directly relates to the individual layers of the solar cell and their properties. The QE for short wavelengths of 300-500 nm is limited by absorption in the window layer stack. As an example it is easy to note that the dotted curve in figure 4.1 is lower than the solid curve in this region. This is a result of the dotted curve having a buffer layer with a lower band gap in this case CdS than the solid curve with a Zn-Sn-O buffer layer. In the middle 500-750 nm region the QE should be high, but can be limited by either reflection of the total stack or by recombination at a place where all of the photo excited electrons pass, as the material interface. In figure 4.1 the cell with the Zn-Sn-O film has an oscillatory behavior in this region indicating that it reflects certain wavelengths more because of interference, a result of a flat interface. In contrast the cell with CdS has flatter QE curve indicating a rougher less reflective surface. At longer wavelengths the QE is possibly lowered by either free carrier absorption or metallic reflection in the heavily doped TCO layer [17]. It might also be possible to indentify if there are problems with either converting longer wavelength photons or collecting their generated free electrons. An indication of this phenomenon is found in figure 4.1 where the average level of the cell with CdS is lower than the cell with Zn-Sn-O for long wavelengths despite using a similar TCO layer. Finally, at some even longer wavelength the QE drops, since the photons at this wavelength or even longer ones do not have enough energy to excite an electron across the

lowest E_g of the CIGS layer. In figure 4.1 both of the curves drop at the same wavelength since they are using similar CIGS. As these examples show QE is a measurement that provides more detailed information about the solar cells compared to the current density values of the JV plot.

It is hard to study the material properties of individual layers and their interfaces for finished solar cells, but there are plenty of methods to analyze these for unfinished cells.

4.3 Optical transmittance and reflectance

Optical transmittance and reflectance are important parameters for layers in a CIGS solar cell. Some layers as the window layer stack are designed to be transparent whereas the CIGS layer should preferably absorb the incident light. It is also beneficial to have a low reflection for these layers, but a high reflection for the Mo back contact as discussed earlier. In this thesis transmittance and reflectance measurements are also used to determine the band gap of thin films through calculating the absorption coefficient, α according to equation 4.1 [37], where d is the film thickness, R the reflectance and T the transmittance at a specific light wavelength.

$$\alpha = -\frac{1}{d}\ln\left(\frac{T}{(1-R)^2}\right) \qquad (4.1)$$

By squaring the absorption coefficient and plotting it versus the energy of the photons it is possible to extrapolate the band gap of the material from the slope of the curve to where the absorption is zero. Similarly to the QE setup the setup for transmittance and reflectance measurement, in this study a Perkin Elmer Lambda 900 dual beam spectrophotometer, uses a light source with a monochromator to be able to measure at specific wavelengths. As for the QE setup it is also possible to sweep the wavelength by controlling the monochromator through a computer. The spectrophotometer in this study uses an integrating sphere which is able to collect light incident from a wide range of angles and guide them to a detector. Transmittance is measured by opening a hole in the sphere and placing the sample in front of the hole. As light is incident on the sample some of the light passes through the sample and is collected by the sphere. It is possible to determine the transmittance of the test sample by relating the measured light intensity signal to a previously measured reference signal without a sample. A key aspect of the transmittance measurement is to have a substrate that is transparent to the wavelengths of interest. Standard SLG is transparent until its band gap of 4.0 eV, whereas fused silica glass has a higher band gap and can therefore be used as a substrate up to at least 4.1eV, which is the highest possible energy of the Lambda 900 instrument. Reflectance is measured in a similar manner as

transmittance, but requires the sample to be moved inside the sphere and placed on the far wall from the opening. As the light passes through the hole in the sphere it goes directly towards the sample on the far wall where part of the light is reflected back into the sphere and is eventually guided to the detector. Due to the nature of the integrating sphere it is possible to collect both the specular and the diffuse light reflection of the film. In this study transmittance and reflectance is measured in paper X for Zn-Sn-O buffer layers on fused silica glass, whereas the entire window layer stack deposited on SLG is measured in paper II. Additionally, the band gap of different (Zn,Mg)O buffer layers deposited on SLG is determined in paper IV and VI. It is however not straight forward to transfer the properties seen for films deposited on glass to films deposited on CIGS, since the initial ALD growth kinetics are quite different between the two surfaces, which in turn might induce differences in the film thickness and composition.

4.4 Other analysis methods

In this thesis several other analysis methods are also used, which provide valuable information about the properties of individual layers or stacks of layers. A detailed discussion of these methods is not within the scope of this thesis, but a list of the methods and in what papers they are used is found in table 4.1.

Table 4.1. *List of additional analysis methods used within this thesis.*

Analysis method	Used in paper	Reference
X-ray fluorescence, XRF	I, III, VII, VIII, IX and X	[38]
X-ray diffraction, XRD	I, II, IV, V, VII, VIII and X	[39]
X-ray reflectivity, XRR	I, VII, IX and X	[39]
X-ray photon spectroscopy, XPS	IV and VIII	[40]
Scanning electron microscopy, SEM	IV and V	[41]
Transmission electron microscopy, TEM	IV, VII and VIII	[42]
Rutherford back scattering, RBS	X	[43]
Hall measurement	VI	[11, 44]

5. Engineering buffer layers

5.1 Band diagram model for a complete $Cu(In,Ga)Se_2$ solar cell

In order to dig deeper into the mechanics of the CIGS solar cells and the importance of the buffer layer it is helpful to study the band diagrams for the typical solar cell stack, shown in figure 5.1.

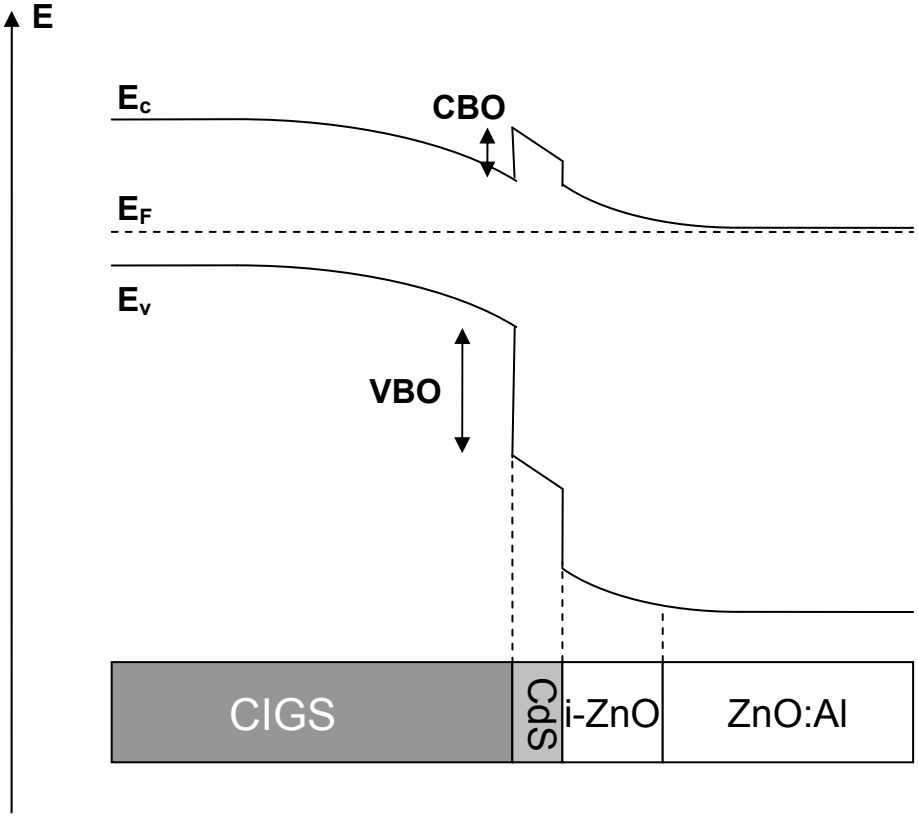

Figure 5.1. Band diagram model for the CIGS solar cell.

A major point of interest in figure 5.1 is the small positive CBO between the CIGS and the CdS buffer layer. At a first glance it might not seem beneficial to introduce a barrier for the electrons to overcome as they are driven towards the n-type ZnO by the electric field in the SCR. However, by ana-

lyzing the position of E_F another interesting aspect becomes apparent, the electrical p-n junction is pushed into the p-type CIGS, which implies that the topmost part of the CIGS is inverted to n-type. Moving the junction into the CIGS and away from the physical material interface reduces the interface recombination [19, 26], since the hole concentration at the interface is reduced. According to a renowned theory [19] it is possible to move the junction into the CIGS by having a zero or a small positive CBO between the absorber and the buffer layer. If the CBO becomes negative the theory predicts that the junction moves towards the physical material interface and the probability for recombination increases, whereas a too large CBO will reduce the probability that the electrons are able to pass the barrier without providing additional energy.

An interesting aspect of CdS that could partially explain its success as a buffer layer is that it seems to have a small positive or zero CBO towards CIGS with a composition corresponding to an x-value of 0.3 [8-10,19]. Since only E_c moves as the band gap or x-value of CIGS changes [13] it is not possible for CdS to maintain a favorable CBO towards the CIGS for all x-values and this might partly explain why neither solar cells with x = 0 or x = 1 achieve the same performance as for x = 0.3 [26]. Interestingly enough CIGS also seem to have the best material properties at x = 0.3 [13, 26], which could further explain why this Ga content works so well.

5.2 Investigation of the conduction band offset using Zn(O,S) buffer layers and $Cu(In,Ga)Se_2$ absorbers with varying compositions

5.2.1 $Cu(In_{1-x},Ga_x)Se_2/Zn(O_{1-z},S_z)$ solar cells

Previous experiments [45] and the results of paper II show that it is possible to use Zn(O,S) as a buffer layer instead of CdS without loosing significant performance for CIGS with x-values of 0.3 if the Zn(O,S) film has a certain S content. It is probable that a Zn(O,S) film with this specific S content forms a favorable CBO towards the CIGS with an x value of 0.3, since E_c of Zn(O,S) varies as a function of the S content according to a previous study [45]. It would thus also in theory be possible to achieve a favorable CBO by changing the Zn(O,S) even for CIGS with x–values that are different from 0.3. It is noteworthy to mention that E_v also moves as the S content changes and that E_g is smaller for intermediate compounds compared to the binary ZnO or ZnS [46]. Additionally, as the S content is increased gradually from ZnO to ZnS, the morphology changes from hexagonal ZnO grains incorporating S to amorphous for intermediate compositions and finally either to hexagonal or cubic ZnS grains incorporating less and less O [45].

The CBO theory is tested experimentally in paper III, paper V and paper VIII where the goal is to optimize the CBO to make good solar cells for all x-values ranging from 0 to 1, by depositing Zn(O,S) buffer layers with z-values that range from 0 to 1. The best performing solar cells for all CIGS compositions are found for the same S content, indirectly determined by XPS and XRD, that gives good performance at x = 0.3. This is interesting since theory predicts that higher S contents would be required to form a favorable CBO when x > 0.3 and similarly that lower S contents would be required when x < 0.3. At the best S content the good results are due to a combination of both high V_{oc} and FF for all of the Ga contents. There is an intermediate maximum for both the FF and the V_{oc} as the S content increases, where the maximum in FF is close to the efficiency maximum while the V_{oc} maximum occurs for higher S contents. In comparison to reference devices with CdS the devices with the best Zn(O,S) layers have comparable or lower efficiency, except for x = 1 and = 0.3 where there is a drastic drop. Breaking it down further with the exception of x = 1, the devices with the best Zn(O,S) layer have lower FF, lower V_{oc} and higher J_{sc} compared to the CdS references, as shown in table 5.1 and figure 5.2a. Figure 5.2b illustrates the corresponding QE measurements and that the increased J_{sc} is partly or completely due to less blue light absorption in the buffer layer as predicted. Additionally, for the intermediate x-values there is an increase in QE for the red and infrared wavelengths.

Table 5.1. *Performance of CIGS solar cells with the best Zn(O,S) buffer layer compared to the reference cells using CdS at Ga contents ranging from 0 to 1.*

V_{oc} [mV]	J_{sc}(QE) [mA/cm^2]	FF [%]	η [%]	Buffer layer	x
423	38.9	69.2	11.4	Zn(O,S)	0
448	37.8	68.3	11.6	CdS	0
507	33.5	67.1	11.4	Zn(O,S)	0.3
575	33.2	73.7	14.1	CdS	0.3
610	29.5	63.9	11.5	Zn(O,S)	0.5
655	25.7	66.2	11.2	CdS	0.5
775	20.4	45.7	7.2	Zn(O,S)	0.75
757	17.0	65.4	8.4	CdS	0.75
726	10.8	49.9	3.9	Zn(O,S)	1
770	13.6	58.9	6.2	CdS	1

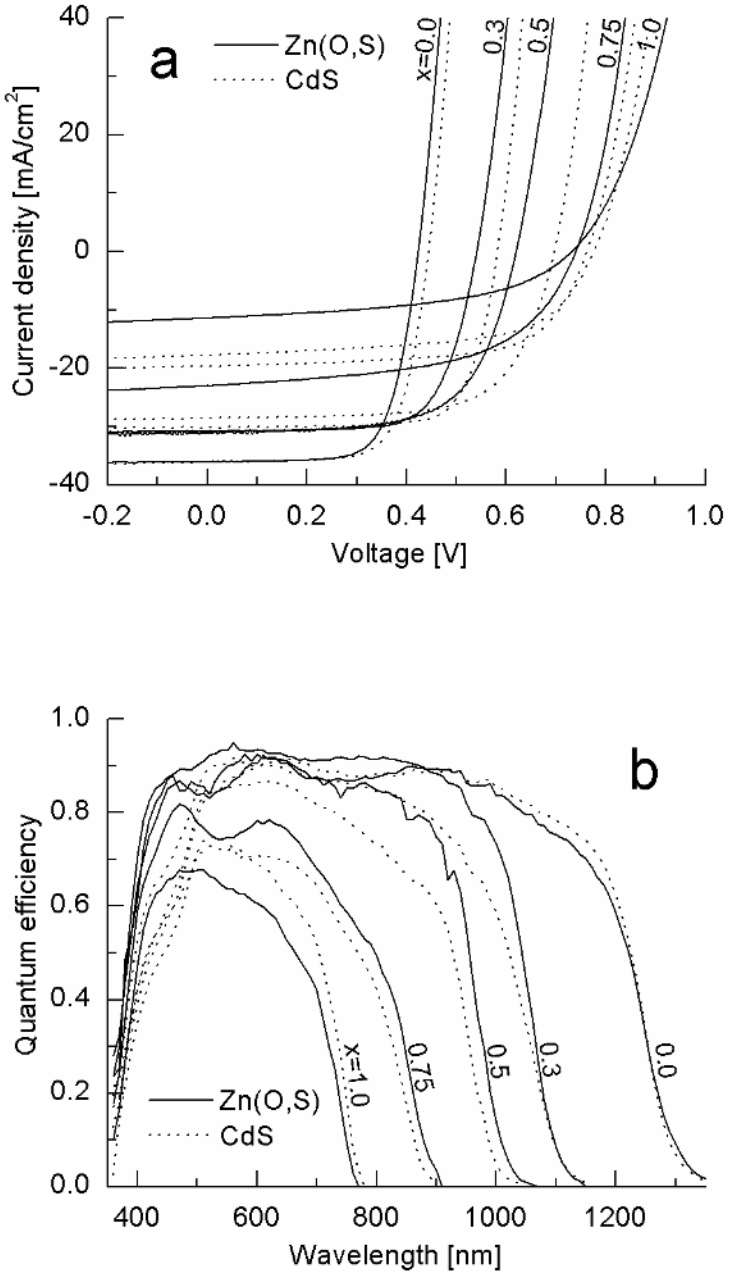

Figure 5.2. a) JV and b) QE of CIGS solar cells with the best Zn(O,S) buffer layer compared to the CdS reference cells, as a function of the CIGS x-value or Ga content.

This could be explained by an increased SCR width in the CIGS allowing for a better collection of the longer wavelengths that are more likely to be absorbed further into the layer. On the other hand a wider SCR also increases the dark current density due to the increased collection of thermally excited electrons which in turn lowers V_{oc}. An indication of this is seen as a tradeoff between V_{oc} and QE for the IR wavelengths as the cells with Zn(O,S) are compared to their CdS references for x = 0, 0.3 and 0.5, where there is hardly any difference in V_{oc} and IR QE for x = 0 but a loss in V_{oc} and a gain in IR QE for the devices with Zn(O,S) at x = 0.5 and 0.3.

5.2.2 Hypothesis of the $Cu(In_{1-x},Ga_x)Se_2/Zn(O_{1-z},S_z)$ interface properties

A hypothesis is suggested in paper VIII to explain the deviation of the results from paper III, paper V and paper VIII compared to the prediction of the CBO theory. The hypothesis is based on observations made on the Zn(O,S) films by TEM, XRD and XPS in paper VIII. XPS results show similar values for the Zn auger parameter of the best Zn(O,S) films for x = 0, 0.3 and 0.75 indicating that the composition remains unchanged in the experiments. For the best Zn(O,S) films the GI-XRD diffractograms show weak hexagonal ZnO peaks slightly shifted towards lower angles, because of the incorporation of S into the lattice. As the S content decreases the peak shift towards ZnO becomes smaller and the peaks grow in intensity indicating less S containing grains and as the S content is increased from the optimal composition the Zn(O,S) films become amorphous in XRD. By using a TEM in scanning mode and moving the beam along a line while measuring EDS, it is possible to measure elemental concentrations along the scanned line. In paper VIII, TEM-EDS scans are performed on the cross section of the solar cells starting in the CIGS, continuing through the Zn(O,S) buffer layer and stopping in the ZnO. The resulting scans from two different positions of the same TEM sample show similar signal intensity of Zn, O and S, except for the region of the Zn(O,S) film that is close to the CIGS/Zn(O,S) interface, where the z-value between the two positions differ. The hypothesis proposes that there is a mixture, as shown in figure 5.3, of hexagonal ZnO phase grains with a negative CBO towards CIGS [45] and a more sulfur rich amorphous phase with a large positive CBO towards CIGS [45] present in the best Zn(O,S) films close to the CIGS interface.

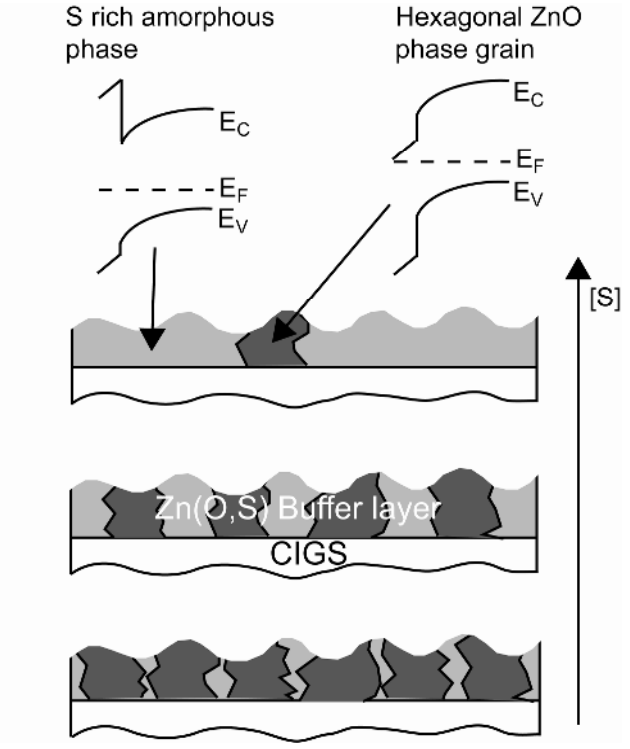

Figure 5.3. Illustration of the local variations in CBO of the Zn(O,S) film at the buffer layer/CIGS interface as proposed by the hypothesis. As the S content of the film increases the hypothesis suggests that there are less of the hexagonal ZnO phase grains and more of the S rich amorphous phase.

Additionally, the ZnO grains are assumed to be good conductors whereas the amorphous S rich phase is assumed to have good electrical surface passivation properties [46]. As the S content increases from ZnO the amount of the conductive grains gradually decreases as illustrated in figure 5.3. This lowers the recombination due to less area with negative CBO and due to a better surface passivation of the S rich phase that also to some extent prevents shunt paths. The result of this is seen as an increase in both FF and V_{oc}. When the S content is increased even further the amount of negative CBO barrier conducting grains that can conduct the current is reduced, while there is more of the high CBO barrier amorphous S-rich phase. As a result the FF drops and finally also the V_{oc} after removing too many or all of the conducting grains. There is thus an optimal S content of the Zn(O,S) buffer layer where both FF and V_{oc} are high that is independent of the band gap of CIGS. This hypothesis would explain the results in paper III, paper V and paper VIII, especially the maxima in FF and V_{oc} mentioned in a previous paragraph and why the CBO theory is not straightforward for cells with two-dimensional variations in material properties.

5.2.3 Dominant recombination path in $CuGaSe_2$/Zn(O,S) solar cells

A different approach to investigate the CBO model is to determine the dominant recombination mechanism for solar cells with a clearly unfavorable CBO such as the best solar cells with x = 1 and Zn(O,S) or CdS found in paper III. By measuring the temperature dependence of the ideal solar cell parameters within a temperature range of 260 – 340 K, it is possible to determine the activation energy, E_a, for the dominant recombination path [47, 48]. As it turns out for x = 1 the CdS cells have both an E_a and a temperature dependence of the other parameters that indicate a space charge region dominated recombination. It is not as straightforward for the Zn(O,S) cells since the E_a indicates that they are dominated by interface recombination, IFR, but the temperature dependence of the other parameters cannot be fitted into any of the existing models [47, 48], possibly indicating that there are multiple types of recombination paths that are comparable in magnitude.

5.2.4 Effect of the CIGS surface roughness

Another example of how the material properties influence the formation of the p-n junction is found in paper V where a temperature profile with a lower temperature in the beginning and a higher temperature at the end is introduced during the CIGS growth in order to control the preferential grain orientation. While previous study showed that certain grain orientations give better solar cell performance [49] the grains in paper V are found to be randomly oriented. However, a more influential side effect of the profiles seems to be that the surfaces of the films become smoother as the starting temperature is lowered, while the grain size as observed by SEM remains unchanged. Comparing the performance of solar cells with Zn(O,S) and their CdS references it is interesting to note that the cells with Zn(O,S) are considerably better in efficiency when the starting temperature is lowered, mainly due to higher J_{sc}. The increase in J_{sc} is seen for both blue wavelengths due to the higher band gap of the buffer layer and for longer wavelengths, probably because of an increased SCR width in the CIGS. For the constant temperature samples the CdS references has a drastic drop in V_{oc} while the cells with Zn(O,S) has a drop in FF, making this the worst temperature profile for both buffer layers.

5.3 (Zn,Mg)O buffer layer properties and how they affect the solar cell performance

5.3.1 Performance of (Zn,Mg)O buffer layers

Earlier studies on (Zn,Mg)O showed that the material can successfully be used as a buffer layer for CIGS solar cells [50, 51], possibly because it is predicted to have a favorable CBO towards CIGS for certain Mg contents. In Paper I the work continues on ALD (Zn,Mg)O buffer layers and sets out to optimize them for an increased solar cell performance. First the CBO is varied by changing E_c of the (Zn,Mg)O films through the Mg content. As is seen in the previous study [50] an E_g of 3.6 eV or a Mg content of 0.2, which would correspond to a CBO of +0.2 eV towards CIGS with a composition corresponding to x = 0.3, is found to give the best performance. Thus, at x = 0.3 the CBO theory seems to be valid, however in paper III the best solar cells for x = 1 are found for the same Mg content of the (Zn,Mg)O films as for those on x = 0.3. Similarly to the Zn(O,S) films deposited on x = 1, it is not possible to determine the dominant recombination type since the data does not fit into any existing model, but the values for E_a suggest interface recombination. The previously suggested hypothesis for Zn(O,S) does not seem to be valid for (Zn,Mg)O because GI-XRD shows that the ALD (Zn,Mg)O retains its hexagonal ZnO phase at these Mg contents [50] and because paper IV shows that this crystalline structure is present even at the interface towards the CIGS.

In comparison to the CdS reference devices solar cells with ALD (Zn,Mg)O are found to be comparable or even better in paper I, paper II and paper IV. Summarized in table 5.2 are the average solar cell parameters from these papers and the champion solar cell with η = 18.1 % (V_{oc} = 668 mV, J_{sc} = 35.7 mA/cm^2 and FF = 75.7 %) from paper II.

Table 5.2. *Performance comparison between solar cells using (Zn,Mg)O buffer layers and their CdS references. Solar cells marked with an asterisk use anti reflective coating.*

Buffer layer	V_{oc} [mV]	J_{sc} [mA/cm^2]	FF [%]	η [%]	x-value	Paper number
(Zn,Mg)O	640	33.7	75.1	16.2	0.3	I
CdS	627	32.2	76.5	15.4	0.3	I
(Zn,Mg)O	748	14.7	56.8	6.2	1	III*
CdS	826	9.7	64.9	5.2	1	III
(Zn,Mg)O	646	34.5	74.0	16.5	0.3	II
CdS	661	33.0	75.1	16.4	0.3	II
(Zn,Mg)O	668	35.7	75.7	18.1	0.3	II, champ*

It is interesting that it is possible to achieve better or comparable performance by replacing CdS with (Zn,Mg)O. CdS is not only predicted to have a favorable CBO for CIGS with x = 0.3, but it also contains both Cd and S that

are considered to be beneficial for a good interface formation towards CIGS. S is believed to electrically passivate bulk defects [52] whereas Cd is predicted to be present in the topmost part of the CIGS layer where it acts as an n-type dopant enhancing the inversion of the p-type CIGS [8-10]. In paper I the best of both worlds is utilized by pretreating the CIGS with either elongated S pulses in the ALD or by a partial Cd electrolyte solution prior to the (Zn,Mg)O buffer layer. Unfortunately, solar cells with a good CIGS material do not improve by these treatments, but an improvement in V_{oc} and FF is seen for cells that have a poor CIGS material.

5.3.2 Influence of thickness and deposition temperature of the (Zn,Mg)O buffer layers

To further improve the performance of CIGS solar cells with (Zn,Mg)O buffer layers, the band gap or the Mg content of the buffer layer is fixed while parameters as thickness and deposition temperature are varied in paper I. As long as the layers are thicker than 70 - 80 nm the solar cell performance seems to be unaffected, even up to thicknesses of 320 nm. If the buffer layers are thinner there is a reduction in both FF and V_{oc}, possibly because of sputter damage from the subsequent ZnO depositions. In paper I the ALD temperature is increased from 105 °C to 180 °C and the resulting solar cell performance is displayed in table 5.3.

Table 5.3. *Solar cell parameters as a function of the (Zn,Mg)O deposition temperature.*

T_{dep} [°C]	V_{oc} [mV]	J_{sc} [mA/cm^2]	FF [%]	η [%]	Resistivity [Ωcm]
105	622	31.6	72.0	14.1	40
120	639	32.6	74.5	15.5	110
135	604	32.1	72.3	14.0	72
150	485	31.9	46.2	7.15	7.4
180	470	31.3	48.4	7.12	0.61
CdS	626	31.6	75.7	15.0	-

The most notable effect of the deposition temperature is the significant drop of about 100 – 200 mV in V_{oc} between the 135 °C cells and the 150 °C cells. In order to find the cause of this drop the cells and the buffer layers are measured by GI-XRD, XPS, TEM, optical transmission and optical reflection in paper IV. Surprisingly, none of these measurements are able to point at any differences between the cells or the buffer layers. On the other hand the measurements do show that the (Zn,Mg)O buffer layers grow as acicular or coconut flake like grains on CIGS, that the films have a uniform composition with respect to the thickness, that the step coverage on the CIGS surface is excellent, that the interface between CIGS and (Zn,Mg)O is sharp or has less than 10 nm of intermixing and as mentioned earlier that the films are

crystalline even at the CIGS/(Zn,Mg)O interface. Surprisingly, differences are however visible in resistivity measurements where the film grown at 135 °C has a resisitivity of 72 Ωcm, an order of magnitude higher than that grown at 150 °C with 7.4 Ωcm. Similar trends in V_{oc} and FF are also found in a previous study where the resistivity of the ALD ZnO buffer layer is intentionally varied [53]. In a cross reference test in paper IV the first tenth of the buffer layer is deposited at a low temperature of 120 °C and the remaining nine tenths at 150 °C. Interestingly enough these cells with η = 14.5 % (V_{oc} = 629 mV, J_{sc} = 32.9 mA/cm^2 and FF = 69.9 %) are close to the 120 °C reference cells with η = 15.0 % (V_{oc} = 631 mV, J_{sc} = 33.3 mA/cm^2 and FF = 71.5 %) and a lot better than the 150 °C reference cells with η = 8.21 % (V_{oc} = 482 mV, J_{sc} = 32.1 mA/cm^2 and FF = 52.9 %). Thus it seems to be crucial for the solar cell performance to have the lower deposition temperature high resistivity film at the interface, but not in the bulk. To get a better picture of the reason behind this further investigations on the topic are required.

5.3.3 Controlling the resistivity of (Zn,Mg)O buffer layers

A previous study [53] suggests that the low resistivity of the higher temperature films is due to O vacancies or Zn interstitials. In order to increase the resistivity of the films while maintaining the deposition temperature an O_2 pulse is added in paper VII after each DEZ/N_2/H_2O/N_2 cycle in the (Zn,Mg)O ALD process. At a growth temperature of 150 °C it is possible to increase the resistivity up to two orders of magnitude by including the extra O_2 pulse and thereby enhance the solar cell performance. However, the best cells at 150 °C do still not perform as well as the reference cells at 120 °C, possibly because the additional O_2 pulse also might oxidize the CIGS surface during the first few growth cycles, which in turn could increase the interface recombination. An experiment that supports this explanation is found in paper VII where a long O_2 pulse is introduced prior to the buffer layer growth, which reduces the performance dramatically, thus there seems to be a trade off between introducing extra O_2 pulses to increase the resistivity and to reduce the pulses to avoid oxidation of the CIGS surface. It is possible that other oxygen sources might give less oxidation and it might also be possible to introduce the additional oxygen later into the buffer layer growth so that it does not oxidize the CIGS, but as previously mentioned it seems to be crucial to have a high resistivity at the interface rather than in the bulk.

5.3.4 (Zn,Mg)O light soaking effects

Another key aspect of CIGS solar cells with (Zn,Mg)O buffer layers is that exposure to light might have a strong influence on their performance. In previous studies and in paper I an increase in FF is observed as these solar cells are subjected to white light for an extended period of time. Typically it

takes 5 to 20 min before the effect saturates and after that it can be retained for several days. One approach to find an explanation to this metastability is to study the (Zn,Mg)O films separately as they are exposed to light. In paper VI we measure a decrease in resistivity that saturates after a few minutes as the (Zn,Mg)O films are exposed to UV light, as shown in figure 5.4. Since the relaxation time of this resistivity change is several days, as is illustrated in figure 5.5, the films are concluded to show persistent photo conductivity, PPC [54, 55].

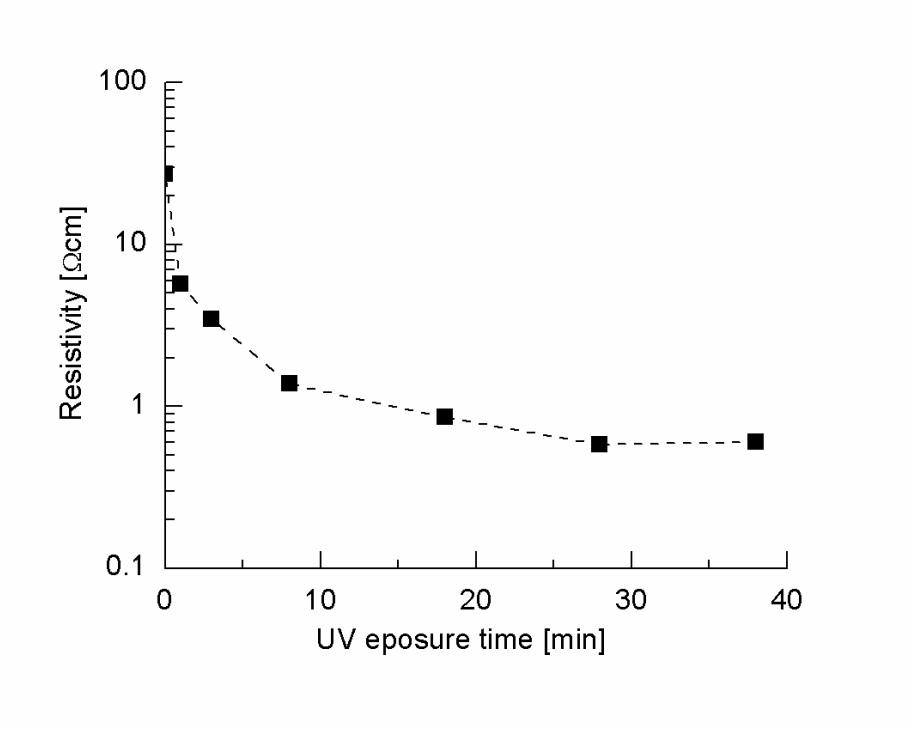

Figure 5.4. Decrease in resistivity as the (Zn,Mg)O film is exposed to UV light soaking.

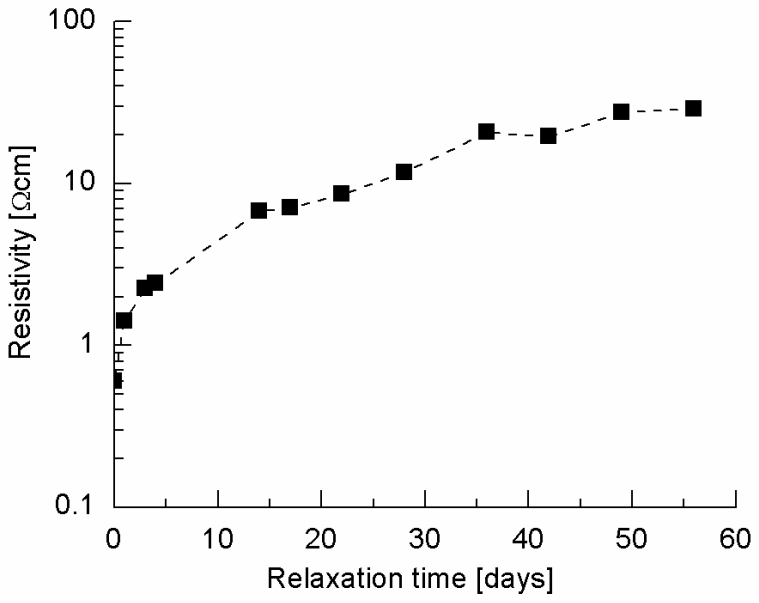

Figure 5.5. Increase in resistivity as the (Zn,Mg)O film is stored in darkness.

Both the decrease in light and the increase in darkness of the resistivity are stronger, up to one order of magnitude, for films with initially high resistivities. The relaxation time is very temperature dependent, measured in days at RT, but shortened to a few hours at an elevated temperature of 100 °C. In paper VI Hall measurements are performed from where it is possible to determine if the changes in resistivity are caused by changes in electron/hole mobility and/or charge carrier concentration. Interestingly enough, the (Zn,Mg)O films show an increase in both carrier concentration and mobility as the resistivity decreases. It is possible that the cause of the increased carrier concentration is due to photoexcitations of deep states localized at defect centers [55,56]. Additionally, the excited defects are believed to slightly rearrange the surrounding crystal lattice [55,56], which could affect and explain the change in carrier mobility as well. For the solar cells, an increased carrier concentration in the buffer layer would induce a stronger band bending in the buffer layer towards the CIGS and thereby lower the effective CBO barrier at that interface [57]. Additionally, it is possible that the increase in mobility also improves free carrier transport through the buffer layer reducing the series resistance of the device. All of these effects would increase the FF and explain the results in paper I. It is harder to explain the results in paper II where solar cells with (Zn,Mg)O buffer layers are sensitive to light soaking if the solar cell has an i-ZnO layer, but not when the i-

ZnO layer is omitted and the initial FF is high. Possibly, the initial effective CBO barrier for the devices without an i-ZnO layer is already low enough to not limit the FF and would therefore not be affected by a further increase in carrier concentration or mobility.

5.4 Zn-Sn-O buffer layers

5.4.1 Properties of Zn-Sn-O thin films by ALD

In paper IX Zn-Sn-O is introduced as a new buffer layer for CIGS solar cells. Previously both ZnO [8-10] and SnO_2 [58] have been used as buffer layers, but the solar cell performance was found to be significantly lower compared to their CdS references. However, the results for SnO_2 buffer layers were high enough to motivate an investigation of the intermediate compounds between ZnO and SnO_x. In paper IX and paper X it is shown that it is possible to grow the intermediate films, denoted as Zn-Sn-O, by using ALD. From XRD measurements in paper X the resulting Zn-Sn-O films are found to be amorphous for most compositions including the pure SnO_x. Towards the other end, close to pure ZnO, weak hexagonal ZnO phase peaks are found with an increased intensity as the Sn content is lowered. It is interesting to study amorphous buffer layers from a strain perspective, since they are not likely to induce any stress because of having a different crystal lattice parameter compared to CIGS. Possibly, this could reduce the amount of recombination centers at the CIGS/buffer layer interface. Optical transmission data of the Zn-Sn-O films deposited on glass show a distinct transmission loss onset for pure ZnO whereas the intermediate compounds and SnO_x show losses that are smeared out over a wider wavelength interval, as seen in figure 5.6. The smeared out losses could possibly indicate that these films are amorphous or that the band gap is indirect.

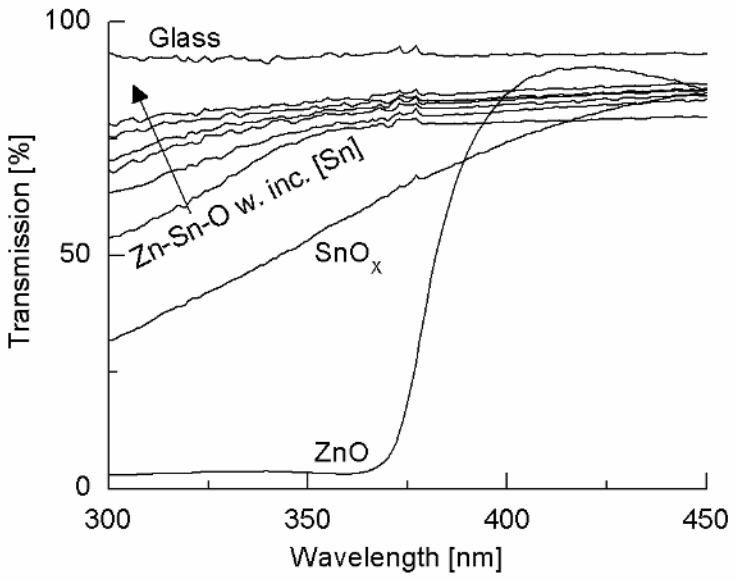

Figure 5.6. Optical transmission as a function of the Sn content of the Zn-Sn-O buffer layers.

Furthermore, a third indication of these films being amorphous is that the density as measured by XRR in paper X goes down for the intermediate compounds compared to ZnO and SnO_x. However, the reduced density could also be an effect of incorporating more hydrogen and ligands into the film during growth of the intermediate compounds. The Sn content of the Zn-Sn-O films as a function of the ALD SnO_x:ZnO cycle ratio is measured by RBS on fused silica/buffer layer stacks in paper X and the resulting values are shown in figure 5.7. The trends in figure 5.7 are that an increased pulse ratio gives an increased Sn content and that a large change in pulse ratio only results in a small change in Sn content for the intermediate compounds. The second trend could possibly be explained by a slower reaction for the tin(IV) dimethylamide precursor on ZnO compared to on SnO_x and similarly by a slower reaction for the DEZ precursor on SnO_x compared to on ZnO. Additionally, the reason for the difference in Sn content compared to the pulse ratio is explained by the reaction speed of tin(IV) dimethylamide on ZnO being slower than the reaction speed of DEZ on SnO_x resulting in a lower Sn content than predicted by the pulse ratio.

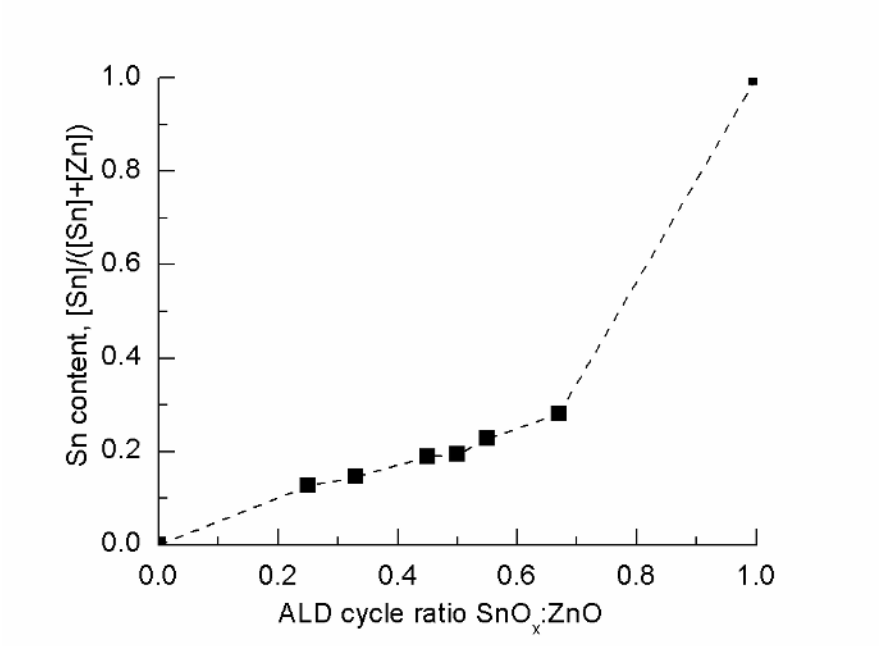

Figure 5.7. Sn content of the Zn-Sn-O film measured on fused silica/Zn-Sn-O stacks by RBS as a function of the ALD SnOx:ZnO cycle ratio.

5.4.2 Zn-Sn-O as a buffer layer in CIGS solar cells

In paper IX and X it is shown that there is an intermediate optimum in solar cell efficiency as the Sn content is increased for the Zn-Sn-O buffer layers due to almost coinciding maxima in both V_{oc} and FF for these contents. Table 5.4 shows the average solar cell performance from paper X as a function of the ALD SnO_x:ZnO cycle ratio.

Table 5.4. *Solar cell parameters from paper X as a function of the ALD SnOx:ZnO cycle ratio.*

Cycle ratio	Thickness [nm]	Voc [mV]	Jsc (QE) [mA/cm2]	FF [%]	η [%]
0	140	383	32.2	58.6	7.2
0.25	97	622	31.9	72.8	14.5
0.33	78	638	32.3	72.4	14.9
0.4	73	647	31.8	72.9	15.0
0.45	69	644	31.9	70.4	14.5
0.5	68	637	31.4	68.2	13.6
0.55	71	638	31.8	65.0	13.2
0.6	71	647	31.9	49.4	10.2
0.67	77	620	31.4	27.5	5.4
1	73	316	30.5	53.8	5.2
CdS	-	649	29.8	72.4	14.0

The average V_{oc} and FF are comparable between the best Zn-Sn-O cells and the CdS references whereas the J_{sc} is increased for Zn-Sn-O layers due to less absorption in the buffer layer and a slightly higher QE for wavelengths longer than 800 nm, as seen in figure 4.1.

It is not straight forward to correlate the results of table 5.4 and figure 5.7, since they are derived from two different series. For the same pulse ratio a ternary film in figure 5.7 is estimated to have a Sn content that is 0.02 higher than for the corresponding ternary film in table 5.4. Taking this into account the best conversion efficiencies of 14-15 % in table 5.4 are found within a relatively narrow Sn content interval of 0.15-0.21. It is possible that the efficiency optimum could be explained by the CBO theory, since certain Sn contents could give favorable CBO. It is however difficult to define E_c for amorphous films and further experiments are therefore required to measure the actual CBO values at the interface. In paper X, the champion CIGS solar cell with a Zn-Sn-O buffer layer has an efficiency of 15.3 % (V_{oc} = 653 mV, J_{sc} = 31.8 mA/cm^2 and FF = 73.8 %) which is comparable to the efficiency of 15.1 % (V_{oc} = 663 mV, J_{sc} = 30.1 mA/cm^2 and FF = 75.8 %) for the champion CdS reference. All of the solar cells with Zn-Sn-O buffer layers in paper IX and X have relatively quick light soaking effects in the order of seconds or at the most minutes and the presented values in this thesis are therefore measured after this light soaking effect has saturated.

5.4.3 Thickness and stability of Zn-Sn-O buffer layers

Since the films become more Sn rich as the film thickness increases the solar cells in paper IX only work for buffer layers that have a thickness of 20-30 nm when they are deposited on glass. Below this thickness interval the solar cells are shunted, possibly because of sputtering damage from the i-ZnO deposition or because of having not completely covering layers. Thicker Zn-

Sn-O films induce blocked JV curves, probably because of the increased Sn content. In contrast, the solar cells in paper X work in a wider range of thicknesses 10 – 80 nm, since they have a constant composition with respect to thickness. On the other hand the long term stability seems to be correlated with the thickness. For thicknesses of 10 – 30 nm the initial values are good, but the performance deteriorates rather quickly, mainly in FF, from lying around in a laboratory environment as seen for all of the devices in paper IX and the devices with thin layers in paper X. It is possible for these devices to recover somewhat through cycled light soaking and annealing, but they are unable to reach their initial performance. Solar cells with 76 nm Zn-Sn-O films also have a FF degradation over time, but recover within a few minutes of light soaking to their original performance as described in paper X. Even after dark dry heat testing at 85 °C for 1000 hours the cells are able to recover from an efficiency of 4-5 % to 14-15 % within a few minutes of light soaking, mainly because of a large improvement in FF as displayed in figure 5.8 a) and b). The successful implementation of the Zn-Sn-O buffer layer both in terms of efficiency and stability makes this an interesting material to study in more detail in future and perhaps implement as a replacement for CdS in industrial processes.

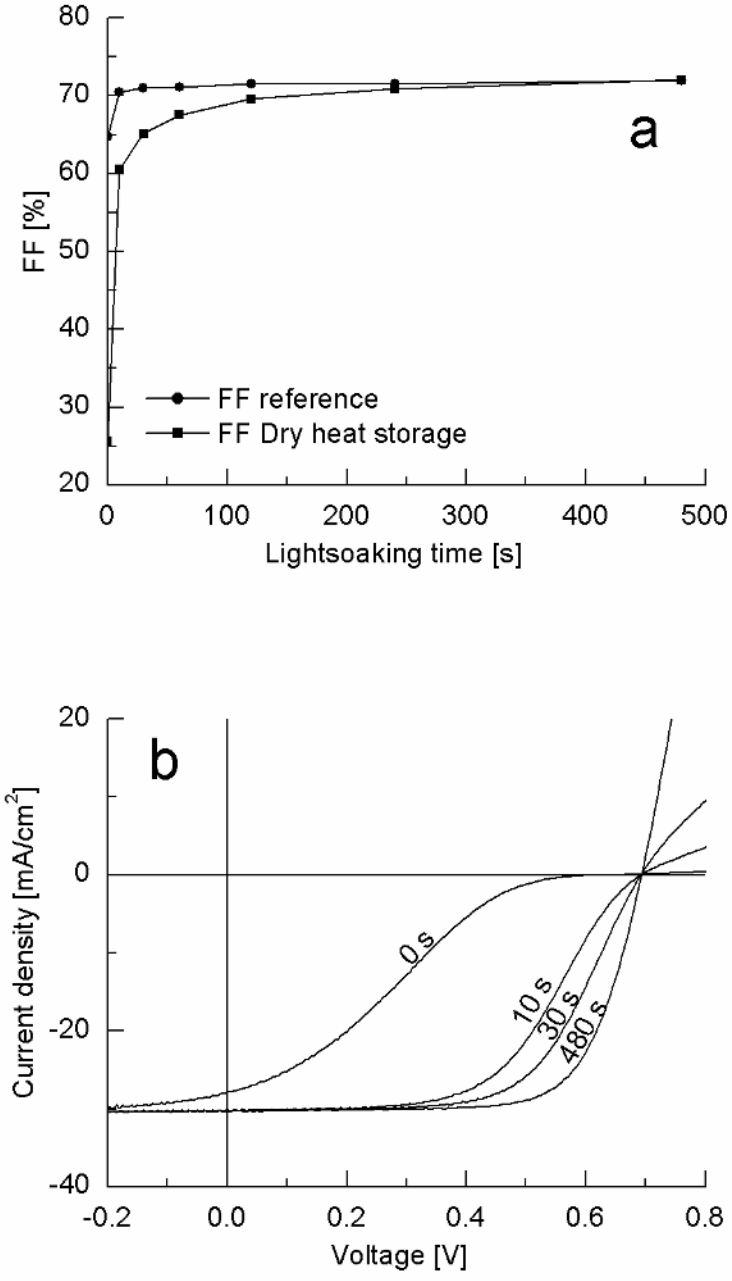

Figure 5.8. a) FF as a function of lightsoaking time for a cell stored in dry heat and for its reference. b) Corresponding JV curves for the dry heat storage cell as a function of the LS time.

5.5 Comparison between the buffer layers

All of the ALD buffer layers Zn(O,S), (Zn,Mg)O and Zn-Sn-O look similar compared to their CdS reference cells in terms of solar cell performance. In general they show lower or comparable V_{oc}, higher J_{sc}, lower FF and lower or comparable η. An example of this is shown in table 5.5 where the best solar cell parameter averages of this thesis are displayed and compared to the CdS reference cells. Light soaking the solar cells improves the FF for all of the buffer layers. The light soaking effect is increased with increasing Mg content for (Zn,Mg)O cells, is strong for Zn-Sn-O cells, is weak for good Zn(O,S) cells and is strong if additional heat is provided for degraded Zn(O,S) cells [59]. Additionally, the effect saturates after a few minutes for Zn-Sn-O films, after 10-20 minutes for Zn(O,S) and (Zn,Mg)O with intermediate Mg contents and after a few hours for (Zn,Mg)O films with higher Mg contents. Solar cells with either (Zn,Mg)O and Zn(O,S) do not generally degrade after storage at room temperature. The solar cells with Zn-Sn-O on the other hand show a severe FF degradation after only a few days of storage at room temperature. It is possible, if the Zn-Sn-O layer is 60-70 nm or thicker, to recover the degraded FF within a few minutes by light soaking. The optimal i-ZnO thickness depends on the buffer layer. An improved performance through an improved J_{sc} and FF is achieved if the i-ZnO layer is omitted for solar cells with Zn(O,S) and (Zn,Mg)O. However, the Zn(O,S) buffer layer requires a thin i-ZnO layer to avoid shunted cells, possibly because it is too thin to prevent the subsequent sputtering from damaging the CIGS surface. A preliminary result shows that omitting the i-ZnO layer for solar cells with a Zn-Sn-O buffer layer increases J_{sc}, but decreases V_{oc} and gives a comparable efficiency.

Table 5.5. *Comparison of the best average solar cell performance for different ALD buffer layers to their CdS reference cells.*

Buffer layer	Paper	V_{oc} [mV]	J_{sc} (QE) [mA/cm^2]	FF [%]	η [%]
Zn(O,S)	II	664	34.8	72.2	16.7
(Zn,Mg)O	II	646	34.5	74.0	16.5
CdS	II	661	33.0	75.1	16.4
Zn-Sn-O	X	647	31.8	72.9	15.0
CdS	X	649	29.8	72.4	14.0

The growth rate of the buffer layers is different. To grow a 50-70 nm thick buffer layer in the same ALD reactor with similar pulse doses requires only 500 cycles of Zn(O,S) compared to 1000 cycles of (Zn,Mg)O and compared to 2000 cycles of Zn-Sn-O. If the precursor is chosen correctly the control of the ALD Zn-Sn-O process is excellent and the same goes for the ALD (Zn,Mg)O process. The ALD Zn(O,S) process is on the other hand harder to control since there are constantly $H_2O + ZnS \Leftrightarrow H_2S + ZnO$ reactions taking place during the H_2O and H_2S pulses. Additionally, the films are

generally more S rich towards the CIGS interface, which probably is a result of multiple effects taking place at the initial growth phase. One possible effect is that the incubation time for growth of ZnO on CIGS is longer than for ZnS on CIGS and another possible effect could be that H_2S pulls oxygen more easily out of the Zn(O,S) film when it has a small bulk volume.

All of the buffer layers have similar morphologies and a similar band gap to ZnO for small incorporations of S, Mg or Sn. As the S content increase the Zn(O,S) buffer layer becomes amorphous and the band gap decreases. The best solar cell performance is achieved for Zn(O,S) buffer layers close to this phase transition where a mixture of crystalline and amorphous phases are present. As the Mg content of the (Zn,Mg)O buffer layer is increased on the other hand the band gap increases, but the hexagonal ZnO phase is retained until a phase mixture of a hexagonal ZnO phase and a cubic MgO phase appears. The best solar cell performance is found for buffer layers that only have the hexagonal ZnO phase present. The Zn-Sn-O buffer layers become amorphous as the Sn-content increase, which makes it hard to define a band gap value, but from optical measurements the effective band gap seems to be larger than for ZnO. The top solar cell performance is achieved for Sn contents that give amorphous Zn-Sn-O buffer layers. It is interesting to note that it is possible to achieve good solar cell performance with buffer layers that are crystalline, amorphous or a mixture of the two.

5.6 Effects of elemental Se at the interface between the buffer layer and the absorber layer

In addition to the CIGS absorber and the buffer layer other materials can unintentionally be present at the interface changing the dynamics of the p-n junction. Oxidation of the CIGS surface was mentioned previously to degrade the performance, implying that the samples should be kept in vacuum, cleaned or processed as soon as possible. Another type of contamination from the laboratory atmosphere is organic carbon compound particles that could introduce states at the interface increasing the recombination current of the devices. Additionally, contamination might arise from the CIGS process chamber itself as in paper IV where crystalline Se is found as two unidentified peaks at 2θ angles 23.4 ° and 29.6 ° in the XRD diffractograms. Since two peaks are not enough to determine a crystalline phase when the CIGS structure is overlapping, Se was evaporated in excess onto the CIGS sample enhancing the weaker characteristic Se peaks enough to appear in the diffractogram. Through measurements of GI-XRD and XPS it became evident that the Se is situated at the surface of the CIGS films. XPS is measured after the ALD of the buffer layers and the subsequent hydrochloric acid etch that selectively removes the ALD layer. For ALD temperatures above 135

°C there was no elemental Se distortion of the $Se3d^{5/2}$ peak and it remained, as illustrated in figure 5.9, at 54 eV, which is the binding energy of Se in CIGS. At lower deposition temperatures a distortion of the $Se3d^{5/2}$ peak is detected that shifts it towards 54.5-55 eV, indicating the presence of elemental Se and since Cu, In and Ga peaks also appeared, the Se crystals are deduced to not form a completely covering layer.

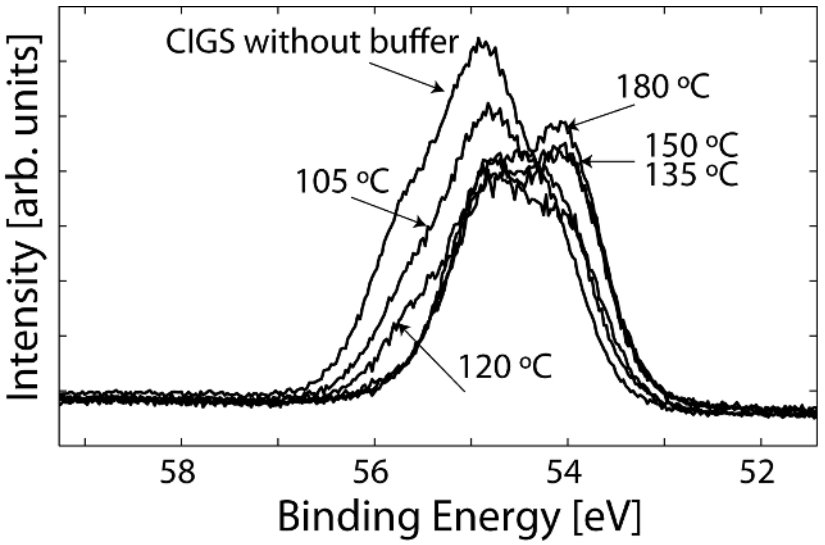

Figure 5.9. Characteristics of the Se3d peak as measured by XPS for samples where the ALD buffer layer has been grown at different temperatures.

GI-XRD verified the presence of crystalline Se even after buffer layer deposition by measuring the peak intensity of (Zn,Mg)O (100), Se(101) and CIGS (112). As the incidence angle is increased there is first an intensity maximum for (Zn,Mg)O (100) followed by a maximum in Se(101) and finally the CIGS (112) signal increases as illustrated in figure 5.10. Elemental Se has a strong effect on the solar cell performance as discussed in a follow up study [60], where small amounts of Se can be beneficial for ALD buffer layers by increasing their FF and V_{oc}, while larger quantities deteriorate J_{sc} due to absorption in the crystalline Se, increases V_{oc} and lowers the FF.

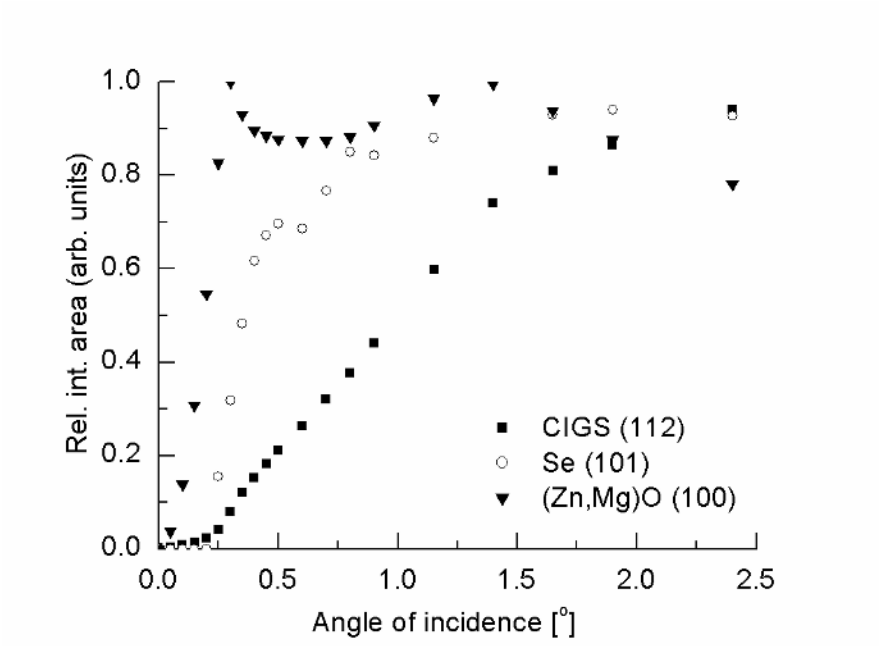

Figure 5.10. Relative peak intensities measured by GI-XRD for the (Zn,Mg)O (100), Se (101) and the CIGS (112) at 2θ-values of 31.7, 29.6 and 26.8 as a function of the angle of incidence.

6. Engineering window layers

6.1 Effects of varying the i-ZnO thickness

As the previous chapter showed, the performance of CIGS solar cells is strongly influenced by the buffer layer properties, since they define the p-n junction. Additionally, as will be discussed in this chapter the buffer layer changes the optimization conditions for the i-ZnO layer in the window layer stack. As mentioned earlier a certain thickness of the i-ZnO layer gave an optimal FF, because it was thick enough to prevent shunt paths and thin enough to avoid a high R_s [33]. In theory it would also be possible to deposit an even thicker buffer layer and omit the i-ZnO, but then more of the incoming photons would be absorbed by the buffer layer if it had a low enough band gap as in the case of CdS. Since the photons that are absorbed in the buffer layer are not collected the current density for the device would decrease as a result of the increased buffer layer thickness. In paper II the need of an i-ZnO layer is discussed when ALD Zn(O,S) and (Zn,Mg)O buffer layers are used. As it turns out the i-ZnO is not needed to prevent shunts for cells with (Zn,Mg)O buffer layers, but a thin layer of 20 – 40 nm is required for the cells with Zn(O,S) buffer layers. While both of the ALD buffer layers have shown excellent step coverage in previous studies [36], it is possible that the thinner Zn(O,S) is not thick enough to prevent the major pinholes or to fully cover the CIGS surface and protect it from subsequent sputter damage. However, the minor FF degradation seen for the CdS references, is not seen for cells with Zn(O,S) or (Zn,Mg)O as the deposition thickness of the i-ZnO is decreased all the way to zero. Instead an increased FF is observed as the thickness decreases generating a top FF of 74 % for the cells with (Zn,Mg)O, but no i-ZnO. In addition to the improved FF for thinner i-ZnO layers the J_{sc} is found to increase in paper II as well. The reason for the improved J_{sc}, is that the i-ZnO has the lowest band gap of the window layers, since the buffer layer band gap of Zn(O,S) and (Zn,Mg)O are higher than that of ZnO and since the highly n-doped ZnO:Al has a Burstein-Moss effect, that effectively increases the band gap as the doping concentration increases. Figure 6.1 illustrates the difference in the ultraviolet and blue QE for solar cells with Zn(O,S) buffer layers and a varying i-ZnO thickness.

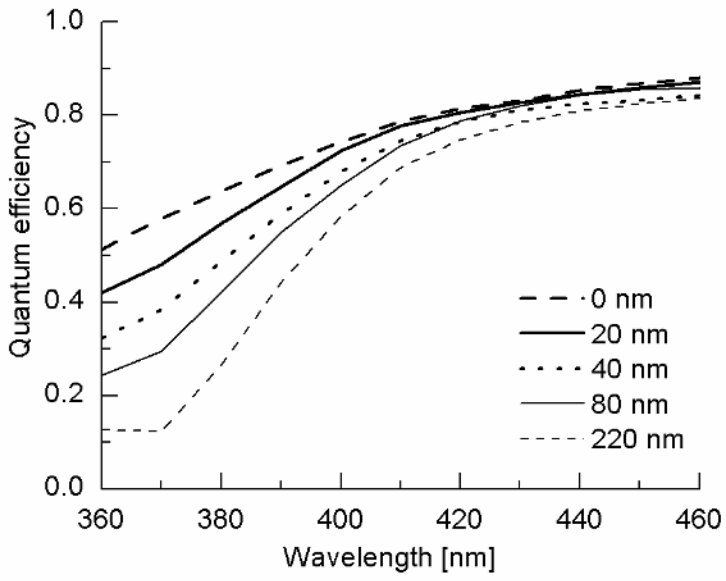

Figure 6.1. QE for solar cells with Zn(O,S) buffer layers as a function of the i-ZnO thickness.

Despite the significant difference in QE for the shorter wavelengths, the change in J_{sc} is small since there are few photons in the solar spectrum in this region [2, 11]. Through omission of the i-ZnO layer and by using anti reflective, AR, coating the champion cell with (Zn,Mg)O of paper II reached an efficiency of 18.1 % (V_{oc} = 668 mV, J_{sc} = 35.7 mA/cm^2 and FF = 75.7 %), which is the highest Cd and S free CIGS solar cell efficiency to date. Paper III also shows an efficiency improvement for x = 1 when the i-ZnO is omitted for solar cells with (Zn,Mg)O buffer layers.

6.2 Buffer layer induced changes in i-ZnO/ZnO:Al crystallinity

Yet another interesting effect that becomes apparent as the window layer stacks are deposited on glass substrates is discussed in Paper II. When the i-ZnO and ZnO:Al are sputtered onto amorphous glass or polycrystalline smooth CdS the crystallinity of the resulting films seems to mostly depend on the parameters of the sputtering process, but when they are deposited on ALD Zn(O,S) and (Zn,Mg)O they inherit some of the crystalline properties of the underlying layer. By using a sufficiently low incidence angle during

GI-XRD it is possible to measure the crystallinity of the i-ZnO and ZnO:Al without measuring the peak intensities of the underlying buffer layer. Figure 6.2 shows the resulting diffractograms of such a measurement for the i-ZnO and ZnO:Al layers as a function of the underlying buffer layer. The most pronounced changes are seen for the intensities of the hexagonal ZnO phase (200), (100), (201) and (101) peaks. It remains to be investigated if these changes are apparent when the i-ZnO and ZnO:Al are sputtered on ALD buffer layers that are deposited onto the rough CIGS surfaces and whether or not these changes in structure are actually affecting the solar cell performance.

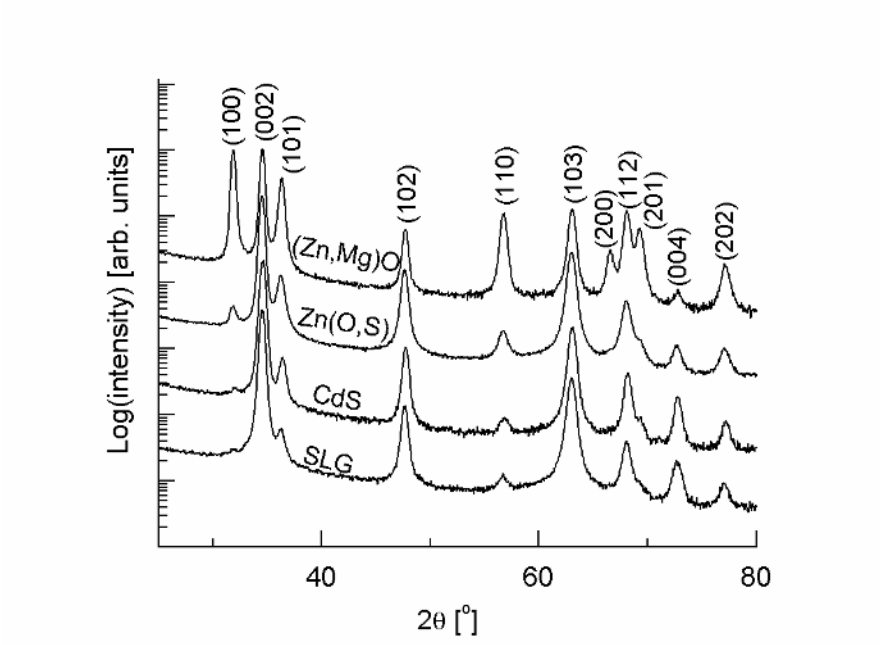

Figure 6.2. GI-XRD diffractograms of glass/buffer layer/i-ZnO/ZnO:Al stacks as a function of the buffer layer. The measurements are performed at a small enough incidence angle to only get peak intensity contributions from the topmost i-ZnO and ZnO:Al layers.

6.3 Replacing the i-ZnO layer with a Zn-Sn-O layer

Earlier studies [61, 62] have shown that the performance of CIGS solar cells improves if the i-ZnO layer is replaced by a sputtered (Zn,Mg)O layer when a CBD ZnS or CdS buffer layer is used. In a small unpublished experiment we investigated if the Zn-Sn-O films exhibit similar properties by replacing the standard CdS and i-ZnO by a thinner CdS and an ALD Zn-Sn-O film. The resulting cells with Zn-Sn-O have η = 14.0 % (V_{oc} = 618 mV, J_{sc} = 31.6

mA/cm^2 and FF = 71.5%) compared to η = 13.4 % (V_{oc} = 620 mV, J_{sc} = 29.4 mA/cm^2 and FF = 73.5 %) of the reference cells using a standard stack. Figure 6.3 shows that the QE is higher for shorter wavelengths for the sample with a Zn-Sn-O layer due to the thinner CdS layer, but also higher for the remaining wavelengths. This could possibly be explained by a lowered interface recombination. Further studies on Zn-Sn-O as a window layer are however required to verify this explanation.

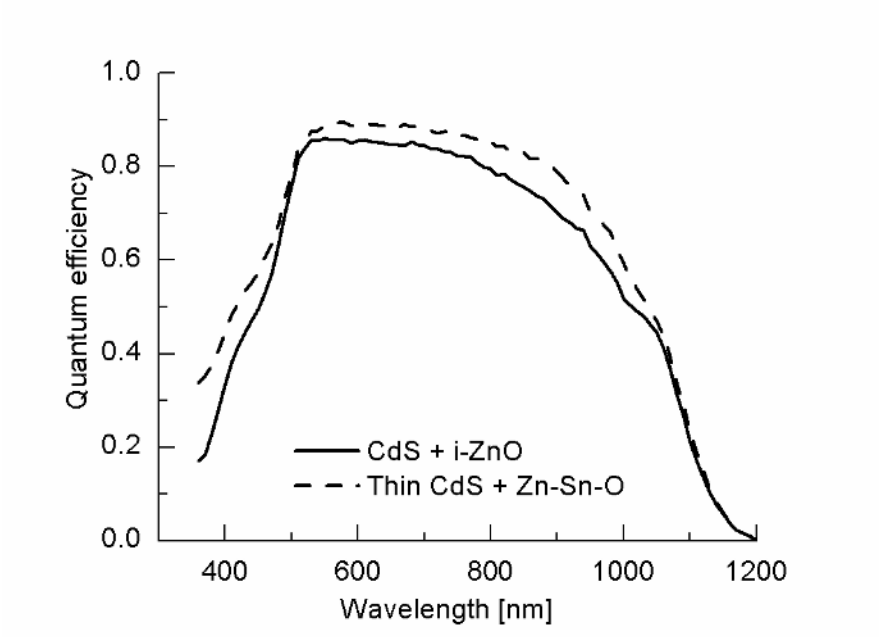

Figure 6.3. Effects in QE as the standard CdS + i-ZnO stack is replaced by a thin CdS + Zn-Sn-O stack.

7. Concluding remarks and outlook

This thesis mainly addresses the impact of replacing the standard CdS buffer layer in CIGS solar cells by an alternative layer that is Cd free. It is an interesting aspect since independently of the CIGS absorber quality the actual formation of the junction and its effects on the solar cell performance are extremely dependent on the buffer layer and to some extent on the following window layers. As an approximation of this dependence the CBO theory predicts that a certain small positive or a zero barrier in the conduction band is crucial in order to form a good p-n junction. CdS buffer layers have favorable CBO towards the most commonly used and highest performing CIGS composition at x = 0.3, but have no ability to change its E_c to match other compositions since it is a binary compound. Zn(O,S), (Zn,Mg)O and Zn-Sn-O have also shown great performance for CIGS compositions with x = 0.3 for certain buffer layer compositions where they are believed to form a favorable CBO. Unlike for CdS it is possible to change E_c of Zn(O,S) and (Zn,Mg)O by changing their compositions and several studies are therefore performed in this thesis with the goal to form a favorable CBO towards other CIGS compositions than x = 0.3 by using these buffer layers. As it turns out and despite having unfavorable CBO according to the CBO theory, the best performance for all x values is found for the same Zn(O,S) buffer layer composition that gives a favorable CBO for x = 0.3. This deviation from the theory indicates a more complicated picture than a one-dimensional model. As an example, measurements performed in this thesis indicates that the best Zn(O,S) films have a phase mixture over the surface of the solar cells of crystalline ZnO grains and S rich amorphous regions close to the CIGS interface. A hypothesis is derived, which claims that a certain mixture of these phases is more important for the performance than forming a favorable average CBO. Additionally, despite of having a favorable CBO other buffer layer properties as the resistivity of (Zn,Mg)O are also crucial for good solar cell performance. A high resistivity of the as grown (Zn,Mg)O film is preferred, especially at the interface towards CIGS, because it is proposed to block the electrical shunt paths that might form at the interface. On the other hand it seems to be beneficial for the FF to reduce this high resistivity by inducing PPC in the buffer layer through lightsoaking after completing the solar cells, possibly because it reduces the effective CBO barrier if it is initially large. In addition to the buffer layers other materials might be deposited at the CIGS surface unintentionally that strongly effect the device performance. In one of

the studies contained in this thesis crystalline Se was found on the surface and later studies showed that a certain amount of Se can actually be beneficial for the solar cell performance. Replacing the buffer layer also changes the optimization conditions for the i-ZnO layer in the window layer stack as seen in this thesis. For (Zn,Mg)O buffer layers an increase in FF is found when the i-ZnO layer is omitted and the best cell with this structure has an efficiency of 18.1 %, a record high for a CIGS solar cell without Cd and S. A main point of the thesis is also the introduction of the new buffer layer Zn-Sn-O that is found to be amorphous in XRD for the top performing material compositions. Using the best Zn-Sn-O buffer layers gives comparable solar cell performance to the reference devices with CdS. Long term stability is still a key issue for these cells, which degrade mainly in FF after dark storage. Thinner films are unable to recover, but thicker films recover after a few minutes of lightsoaking.

Looking ahead, as the market for CIGS solar cells keeps growing and the looming threat of a world wide ban of Cd in electronics remains present, alternatives to the CdS layer will keep on being an interesting topic for research. In particular the buffer layer material properties seem to be one of the keys for good performance and a natural step would therefore be to continue studying the material properties and add to the already elaborate work that has been performed in this field for Zn(O,S) and (Zn,Mg)O. It is still too early to predict the future for the Zn-Sn-O buffer layer, but the initial results are very promising and a patent is already in the making. Further studies on Zn-Sn-O as a buffer layer could also provide valuable information for the general understanding on the buffer layer/CIGS interface. As new absorber layers like Cu_2ZnSnS_4 emerge to replace amorphous Si, CIGS and CdTe the need for a Cd-free buffer layer to define the p-n junction will remain and since Zn(O,S), (Zn,Mg)O and Zn-Sn-O are so versatile it would not be surprising if the solar cell related interest in these materials were to outlive that of CIGS itself.

Summary in Swedish

Hur kadmiumfria buffertlager och deras materialegenskaper påverkar prestanda hos $Cu(In,Ga)Se_2$ solceller

Solen är en enorm källa för energi och även om bara en bråkdel av dess genererade effekt når Jorden räcker den till för att försörja det mänskliga behovet flera gånger om. För att kunna ta till vara på den instrålade effekten behövs något som absorberar solljuset och omvandlar det till något som kan utnyttjas i dagligt bruk som t.ex. värme eller elektricitet. En solcell är en enhet som omvandlar just ljus direkt till elektricitet utan några mellansteg, vilket gör solceller till en intressant typ av kraftverk för produktion av förnybar energi. Intresset är idag så stort att marknaden för solcellsinstallationer växer med 40 % per år. Eftersom många företag vill komma in på en sådan lukrativ marknad produceras det just nu mer solceller än vad som efterfrågas på markanden. Detta gör att produktionsföretagen tvingas pressa sina priser på solceller för att kunna konkurrera om kunderna. Ett sätt att pressa priset är att använda mindre av de dyra materialen i solcellen och detta har lett till en utveckling av tunnfilmssolceller, där solcellen består av ett antal tunna filmer som totalt sett endast är ett par μm tjocka och där en millimetertjock billig glasskiva, plast eller metallfolie används för att bära den sköra strukturen. Ett av de intressanta tunnfilmsmaterialen som även behandlas i den här avhandlingen och som så här långt har visat den högsta solcellsverkningsgraden på forskningsnivå är $Cu(In,Ga)Se_2$, CIGS.

I korthet konstrueras en solcell av två halvledare, en av så kallad n-typ som har ett överskott av termiskt exciterade elektroner i det så kallade ledningsbandet jämfört med ett idealt material och en av p-typ som har ett underskott av termiskt exciterade elektroner i ledningsbandet, men som har ett överskott av tomma energitillstånd, hål, i det så kallade valensbandet. Vid gränsen mellan dessa material skapas ett elektriskt fält i solcellen som driver elektronerna och hålen mot respektive längsmed fältriktningen, men utan pålagd spänning över solcellen kompenseras denna effekt av elektrondiffusion och nettoströmmen är noll. Fältet skapar dessutom en skillnad i energi för elektronerna i ledningsbandet mellan n- och p-typ materialet. När ljuset kommer i små energipaket kallade fotoner till solcellen kan de absorberas av elektroner som då exciteras. De ljusexciterade elektronerna drivs av det

elektriska fältet och skapar en nettoström i solcellen om den ansluts till en elektrisk last och kan då leverera en elektrisk effekt.

Eftersom det är svårt att göra stabil n-typ CIGS krävs fler material för att skapa solcellen, samtidigt är det önskvärt rent prestandamässigt att absorbera allt ljus i CIGS skiktet. Därför finns det som standard ett antal n-typ material som är transparenta för synligt ljus i CIGS solceller, så kallade fönsterlager, som fulländar p-n övergången. Ett av lagren måste dessutom agera som en elektrisk kontakt och det är därför vanligt att en transparant ledande oxid som ZnO väljs för detta ändamål. Tyvärr skapar ZnO ett abrupt negativt steg i ledningsbandet när det är i kontakt med CIGS, vilket enligt teorin ökar den så kallade gränsskiktsrekombinationen som försämrar solcellens prestanda. Det är därför standard att inkludera ett tunt skikt av CdS som visserligen absorberar en del av det blå och ultravioletta solljuset, men som inte har eller har ett litet positivt steg i ledningsbandet sett från CIGS, vilket ger en mindre gränsskiktsrekombination. Eftersom Cd är giftigt och CdS absorberar en del av solljuset är det intressant att ersätta detta lager, även kallat buffertlager, med ett annat giftfritt material som ger lika bra eller bättre prestanda, vilket är ett av huvudmålen i den här avhandlingen.

Tidigare har både Zn(O,S) och (Zn,Mg)O buffertlager belagts genom atomlagerdeponering, ALD, och använts i CIGS solceller istället för CdS utan att förlora prestanda. Under ALD introduceras varje ämne sekventiellt genom en bärgas till provet. För att undvika de höga temperaturer som krävs för att förånga t.ex. metaller sänks ångtrycket för dessa genom att binda dem till olika kolföreningar eller grundämnen och formera en så kallad precursor. När precursorn når provet reagerar kolföreningarna med ytan, vilket förhoppningsvis leder till att deponeringsämnet binder med ytan. Denna effekt saturerar när det inte längre finns någon oreagerad yta kvar att tillgå på provet och det har nu löst definierat bildats ett atomlager på provet. Allt som inte ingår i det första lagret blåses bort med en ren bärgaspuls. För att skapa ett sammansatt material introduceras en annan precursor efter det i bärgasflödet som reagerar med det första lagret på ett liknande sätt tills reaktionen saturerar. Slutligen följs detta av ytterligare en sköljpuls med bärgas som därmed kompletterar en så kallad processcykel i ALD. Genom att låta varje pulseffekt saturera och genom att kontrollera antalet cykler fås en utmärkt kontroll på både filmtjocklek och sammansättning även på väldigt ytojämna substrat som t.ex. CIGS.

Den här avhandlingen fortsätter arbetet med Zn(O,S) och (Zn,Mg)O buffertlager, genom att ta reda på vilka materialegenskaper som är viktiga för en hög solcellsprestanda. Som det tidigare nämndes är det fördelaktigt att ha ett litet steg i ledningsbandet mellan CIGS och buffert lagret för att minska gränsskiktsrekombinationen, men en allt för hög barriär kommer enligt teorin att blockera de exciterade elektronerna och därmed försämra solcellens prestanda. Normalt sett används ett CIGS lager med en galliumhalt som ger ett bandgap på 1.1 eV för produktion av solceller. Enligt teorin borde ett

större bandgap vara bättre, vilket är möjligt att åstadkomma genom att öka galliumhalten i CIGS materialet. Samtidigt som galliumhalten ökar så förflyttas ledningsbandet i CIGS materialet till högre nivåer, vilket gör att CdS materialet som har en fast ledningsbandsnivå kommer att formera ett ofördelaktigt negativt steg mot CIGS materialet. För Zn(O,S) är det möjligt att variera ledningsbandets nivå med hjälp av materialets svavelhalt, vilket gör det möjligt att formera fördelaktiga steg i ledningsbandet även för CIGS med hög galliumhalt. I den här avhandlingen visas resultatet av en studie där både galliumhalten i CIGS materialet och svavelhalten i Zn(O,S) buffertlagret ändras. Överraskande nog fungerar en viss svavelhalt bäst för alla galliumhalter av CIGS materialet trots att det rent teoretiskt inte borde vara fördelaktigt. Vid en närmare analys genom röntgendiffraktion, elektronmikroskopi och elektronspektroskopi upptäcktes att Zn(O,S) har tvådimensionella variationer i svavelinnehållet nära CIGS ytan, vilket betyder att det lokalt finns variationer i ledningsbandssteget. En hypotes har därför föreslagits i den här avhandlingen som bygger på analysen och som förklarar de överraskande resultaten. Hypotesen beskriver att det är fördelaktigt att ha en viss blandning av områden med en hög svavelhalt som har bra elektriska passiveringsegenskaper och områden med en låg svavelhalt som har bra elektrisk ledningsförmåga oavsett vilken galliumhalt som CIGS materialet har.

I avhandlingen optimeras även (Zn,Mg)O buffertlager för att ge så bra solcellsprestanda som möjligt. Förbehandlingar av CIGS skiktet med Cd och S innan (Zn,Mg)O deponeringen gör dåliga solceller bättre, men ger inte en ökad prestanda för bra celler. Tjockleken av (Zn,Mg)O buffertskiktet har inte någon inverkan på solcellerna så länge de är tjockare än 70 nm, men för tunnare lager minskar öppenkretsspänningen, V_{oc}, och fyllnadsfaktorn, FF. Om deponeringstemperaturen för (Zn,Mg)O ökas till över 135 °C minskar V_{oc} drastiskt, vilket efter en omfattande analys kunde härledas till en minskad resistivitet i (Zn,Mg)O filmen. Även om det är fördelaktigt för solcellen att ha en hög resistivitet för det deponerade buffertlagret, förmodligen för att det hindrar läckströmmar, så verkar cellens prestanda bli ännu bättre om filmernas resistivitet sänks genom belysning i en efterbehandling. Under belysningen induceras långvarig fotokonduktivitet i (Zn,Mg)O filmerna som gissningsvis sänker det effektiva steget i ledningsbandet så att celler där steget initialt sett är högt får ett effektivt sett lägre steg och därmed en bättre FF.

Den här avhandlingen introducerar även Zn-Sn-O som ett nytt buffertlagermaterial för CIGS solceller. För en viss sammansättning på Zn-Sn-O buffertlagret är solcellsverkningsgraden jämförbar gentemot CdS referenscellerna. Tjockare Zn-Sn-O filmer verkar ha bättre solcellsstabilitet jämfört med tunnare filmer. Till sist beror processkontrollen starkt på vilken typ av tennkemikalie som används under tillväxten.

Genom att byta ut CdS buffertlagret i solcellen ändras även optimeringsvillkoren för de andra ZnO fönsterlagren. Ett av dessa ZnO lager

med hög resistivitet deponeras normalt sett ovanpå CdS för att hindra de eventuella läckströmmar som CdS inte klarar av att hindra själv. De alternativa buffertlagren som beläggs genom ALD är däremot bättre på att hindra dessa läckströmmar och som en studie i den här avhandlingen visar så behövs därmed inte det högresistiva ZnO, i-ZnO, lagret om ett (Zn,Mg)O buffertlager används och endast ett tunt skikt räcker för solceller med ett Zn(O,S) buffertlager. FF och kortslutningsströmtätheten, J_{sc}, ökar dessutom som en bonus av tjockleksreduktionen eller utelämnandet av det i-ZnO skiktet för cellerna med Zn(O,S) och (Zn,Mg)O. Som en följd av att utelämna i-ZnO lagret uppnåddes en högsta verkningsgrad på 18.1 % för en solcell med ett (Zn,Mg)O buffertlager, vilket är den bästa verkningsgraden hittills för en Cd och S fri CIGS solcell.

För att sammanfatta så är det möjligt att uppnå samma solcellsprestanda med Zn(O,S), (Zn,Mg)O och Zn-Sn-O buffertlager som för CdS om de har fördelaktiga materialegenskaper. Det är också viktigt att inte glömma bort att optimera om de andra lagren i solcellen vid byte av buffertlager, eftersom det kan höja solcellens prestanda. Eftersom buffertlagret och dess egenskaper är så kritiskt för solcellens prestanda, eftersom nya solcellsmaterial förmodligen kommer att kräva buffertlager och eftersom ett Cd-förbud alltid är överhängande är det väldigt troligt att forskningen på dessa Cd fria buffertlager kommer att fortsätta långt efter det att denna avhandling har publicerats.

Acknowledgements

My supervisor in chief Charlotte deserves an enormous thank you for being around even when she is not at Ångström, for her constant ability to come up with dozens of useful literature, for her direct answers, her practical and theoretical knowledge about buffer layers, her ability to sit down and listen and discuss almost whenever, her efficiency and her constant interest in my projects.
Big thanks also go to the lone chemist Tobias for being my second in command supervisor, giving me thought trough feed back about my projects, being around for discussions (whenever you got up back in the day), trying to teach me chemistry and giving me invaluable lessons on how to slack at the university. Also thanks for the many not so serious discussions about a certain theoretician, gold diggers, devious schemes, politics and energy stealing theory.
Special thanks go to Marika for being my senior supervisor, group leader and taking care of all the PR, bureaucratic paperwork, making us heard at various important meetings and for taking care of the cumbersome funding issues with those who will not be named so that the rest of us can work in relative peace. On a more scientific level I am thankful for her excellent knowledge about CIGS and her memory of long forgotten studies that has stopped me from repeating someone else's work.
Thank you Uwe Zimmermann for being my non official supervisor and providing me with countless hours of advice and help concerning science and broken equipment. Thanks for all those events outside/after work and being a pan narran about old and modern electrical technology, trips and chili peppers.
I would also like to thank my brother in angst ("work") Per-Oskar for putting up with me in the tundra room, teaching me about the wonderful worlds of stability and module patterning and for trading cynical remarks about the world, Ny-Teknik articles and the university. Bonus thanks for his interest in and ability to recite American cartoons and for introducing Jonathan Coulton songs and fail blog to me.
Jonas deserves big thanks for his outstanding work on the modeling of the CIGS solar cells, I would have been lost in silly presumptions based on statistically shaky experiments were it not for his models. I am also thankful for his interest in absurd Swedish humor, so that I have someone to discuss the silliness with.

I thank Sebastian for his knowledge about CIGS and especially the BAK (even though it has been "long time" since I last ran it, rate plots on paper long), his knowledge about the back contact and his constant willingness to help out. Additional, thanks for providing information about the current affairs in Germany and for introducing me to Dilbert and Ph.D. comics back when we were sharing a desk in the office space.
Thank you Timo for your invaluable knowledge about electron microscopy, for your professional attitude towards work and for joining the right group (oopsie!). Also thanks for dragging me to a party every once in a while I really appreciate it.
I would also like to thank Jonathan for bringing us some CuZnSnS knowledge, Johan for taking over my IEA-PVPS work, Piotr for returning to the scene of the crime, Hendrik for joining up for innebandy and Mukes for bringing in some very attractive magnetic ideas.
Thanks to the people that are no longer with us (but not dead) as Martha Ruth for providing huge amounts of world class CIGS, Einar Söderström for sputtering countless of Mo substrates for my erratic CGS series and Jens Schöldström for his information regarding the CUPRO process and for his provocative statements, funny stories and for being "such a good sport".
The remaining part of the division deserves a thank you as well and especially Marianne who keeps the crazy scientists at bay and who has to deal with the seemingly endless bureaucratic changes that are thrown on us every year. Also big thanks to Iliya for taking care of the division during my first years and to Shi Li for his present care of the division. Jörgen also deserves a thank you for fighting for the Ph.D. students' wellbeing at the university and for providing a little piece of "bästsidan" to the division. Thank you Herman for your input on my semiconductor problems and for telling us stories about Uppsala in the past.
I thank the Friday beer crew for providing company, discussions and ideas about almost anything in between heaven and earth, especially Wolfgang for still joining us every now and then with your stories and knowledge of the past.
Thank you Solibro employees for being helpful with equipment maintenance and for letting me jump in with some measurements every now and then and special thanks to Erik and Uwe Seeber for a fun time when we shared an office space.

I also thank my parents from the bottom of my heart for supporting and caring throughout all of the almost thirty years now. I also thank the rest of my relatives for still talking to me after I have been missing a lot of the big occasions for almost 7 years now, sorry, hopefully things will improve in the future. I also send a thank you across the pond to my slightly more distant relatives that still keep in contact with me.

And thank you my wonderful friends from old and new that might be far away on the map, but who always bring a smile back on my face when ever I see or hear from you.
Also thanks to the remaining people that I have forgotten to mention (even to those teachers who did not believe in me, it just made me keener to prove you wrong) who brought me to where and made me who I am today, it was a long road but it was worth it.

References

1. D. Williams, Sun Fact Sheet, retrieved 2010-09-13 from NASA's webpage: http://nssdc.gsfc.nasa.gov/planetary/factsheet/sunfact.html.
2. M. Green, Solar Cells: Operating Principles, Technology and System Applications, 1992, The University of New South Wales: Rosebery.
3. K. Chorpa and S. Das, Thin Film Solar Cells, 1983, Plenum: New York.
4. D. Chapin, C. Fuller and G. Pearson, A new silicon p-n junction photocell for converting solar radiation into electrical power. *Journal of Applied Physics*, 25 (1954) p. 676-677.
5. M. Green, K. Emery, Y. Hishikawa and W. Warta, Solar cell efficiency tables (version 36), *Progress in Photovoltaics: Research and Applications*, 18 (2010) p. 346-352.
6. International Energy Agency Photovoltaic Power Systems Programme Task 1, Trends in photovoltaic applications: Survey report of selected IEA countries between 1992 and 2009, available online at www.iea-pvps.org.
7. European parliament, Directive 2002/95/EC, available online at http://europa.eu.int.
8. N. Naghavi, D. Abou-Ras, N. Allsop, N. Barreau, S. Bücheler, A. Ennaoui, C.-H. Fischer, C. Guillen, D. Hariskos, J. Herrero, R. Klenk, K. Kushiya, D. Lincot, R. Menner, T. Nakada, C. Platzer-Björkman, S. Spiering, A.N. Tiwari and T. Törndahl, Buffer layers and transparent conducting oxides for chalcopyrite $Cu(In,Ga)(S,Se)_2$ based thin film photovoltaics: present status and current developments, *Progress in Photovoltaics: Research and Applications*, 18 (2010) p. 411-433.
9. S. Siebentritt, Alternative buffers for chalcopyrite solar cells, *Solar Energy*, 77 (2004) p.767-775.
10. D. Hariskos, S. Spiering and M. Powalla, Buffer layers in $Cu(In,Ga)Se_2$ solar cells and modules, Thin Solid Films, 480-481 (2005) p. 99-109.
11. S. Sze, Semiconductor devices: Physics and Technology, 2nd Edition, 2002, Wiley: New York.
12. U. Malm, Modelling and Degradation Characteristics of Thin-Film CIGS Solar Cells, Ph.D. Thesis, Department of Engineering Sciences, 2008, Uppsala University, Uppsala.
13. S. Siebentritt, M. Igalson, C. Persson and S. Lany, The electronic structure of chalcopyrites—bands, point defects and grain boundaries, *Progress in Photovoltaics: Research and Applications*, 18 (2010) p. 390-410.
14. C. Hibberd, E. Chassaing, W. Liu, D. Mitzi, D. Lincot and A. Tiwari, Non-vacuum methods for formation of $Cu(In, Ga)(Se, S)_2$ thin film photovoltaic absorbers, *Progress in Photovoltaics: Research and Applications*, 18 (2010) p. 434-452.
15. S. Niki, M. Contreras, I. Repins, M. Powalla, K. Kushiya, S. Ishizuka and K. Matsubara, CIGS absorbers and processes, *Progress in Photovoltaics: Research and Applications*, 18 (2010) p. 453-466.

16. V. Mitin, V. Kochelap and M. Stroscio, Quantum Heterostructures: Microelectronics and Optoelectronics, 1999, Cambridge University Press: Cambridge.
17. N. Ashcroft and I. Mermin, Solid State Physics, 1976, Holt, Reinhart and Winston: Ne York.
18. G. Somorjai, Introduction to surface chemistry and catalysis, 1994, Wiley: New York.
19. A. Niemegeers, M. Burgelman and A. De Vos, On the CdS/$CuInSe_2$ band discontinuity, *Applied Physics Letters*, 67 (1995) p. 843-845.
20. T. Nakada, Nano-structural investigations on Cd-doping into Cu(In,Ga)Se_2 thin films by chemical bath deposition process, *Thin Solid Films*, 361-362 (2000) p. 346-352.
21. J. Kessler, K. Velthaus, M. Ruckh, R. Laichinger, H. Schock, D. Lincot, R. Ortega and J. Vedel, Chemical bath deposition of CdS on $CuInSe_2$, etching effects and growth kinetics, *Proceedings of the 6th International Photovoltaic Science and Engineering Conference*, 1992 p. 1005-1009.
22. K. Ramanathan, R. Bhattacharya, J. Granata, J. Webb, D. Niles, M. Contreras, H. Wiesner, F. Hasoon and R. Noufi, Advances in the CIS research at NREL, *Proceedings of the 26th IEEE Photovolataic Specialists Conference*, 1997 p. 319-322.
23. U. Rau, K. Taretto and S. Siebentritt, Grain boundaries in Cu(In,Ga)(Se,S)$_2$ thin-film solar cells, *Applied Physics A*, 96 (2009) p. 221-234.
24. J. Kessler, M. Bodegård, J. Hedström and L. Stolt, Baseline Cu(In,Ga)Se_2 device production: Control and statistical significance, *Solar Energy Materials and Solar Cells*, 67 (2001) p. 67-76.
25. W. Shafarman and L. Stolt, Cu(In,Ga)Se2 solar cells, in: S. Hegedus and A. Luque, Handbook of Photovoltaic Science and Engineering, 2003, John Wiley and Sons Ltd.: West Sussex.
26. R. Herberholz, V. Nadenau, U. Rühle, C. Köble, H. Schock and B. Dimmler, Prospects of wide-gap chalcopyrites for thin film photovoltaic modules, *Solar Energy Materials and Solar Cells*, 49 (1997) p. 227-237.
27. O. Lundberg, Band Gap Profiling and High Speed Deposition of Cu(In,Ga)Se_2 for Thin Film Solar Cells, Ph.D. Thesis, Department of Engineering Sciences, 2003, Uppsala University, Uppsala.
28. K. Ramanathan, M. Contreras, C. Perkins, S. Asher, F. Hasoon, J. Keane, D. Young, M. Romero, W. Metzger, R. Noufi, J. Ward and A. Duda. Properties of 19.2% efficiency ZnO/CdS/$CuInGaSe_2$, thin-film solar cells, *Progress in Photovoltaics Research and Applications*, 11 (2003) p.225–230.
29. J. Schöldström, U. Zimmermann and M. Edoff, Dynamic radiative properties of the Cu(In,Ga)Se_2 layer during the co-evaporation process, *Progress in Photovoltaics Research and Applications*, 18 (2010) p. 321-327.
30. I. Repins, M. Contreras, B. Egaas, C. Dehart, J Scharf, C. Perkins, B. To and R. Noufi, 19.9%-efficient ZnO/CdS/Cu(In,Ga)Se_2 solar cell with 81.2 % fill factor, *Progress in Photovoltaics Research and Applications*, 16 (2008) p. 235-239.
31. J. Kessler, C. Chityuttakan, J. Lu, J. Schöldström and L. Stolt, Cu(In,Ga)Se_2 thin films grown with a Cu-poor/rich/poor sequence: growth model and structural considerations, *Progress in Photovoltaics: Research and Applications*, 11 (2003) p. 319-331.
32. M. Edoff, S. Woldegiorgis, P. Neretnieks, M. Ruth, J. Kessler and L. Stolt, CIGS submodules with high performance and high manufacturability, *Proceedings of the 19th European Photovoltaic Energy Conference and Exhibition*, Paris, (2004) p. 1690-1693.

33. S. Ishizuka, K. Sakurai, A. Yamada, K. Matsubara, P. Fons, K. Iwata, S. Nakamura, Y. Kimura, T. Baba, H. Nakanishi, T. Kojima and S. Niki, Fabrication of wide-gap Cu(In1-xGax)Se_2 thin film solar cells: a study on the correlation of cell performance with highly resistive i-ZnO, *Solar Energy Materials and Solar Cells*, 87 (2005) p. 541-548.
34. R. Puurunen, Surface chemistry of atomic layer deposition: A case study for the trimethylaluminium/water process, *Journal of Applied Physics*, 97 (2005) p. 12301-1-52.
35. E.B. Yousfi, B. Weinberger, F. Donsanti, P. Cowache and D. Lincot, Atomic layer deposition of zinc oxide and indium sulfide layers for Cu(In,Ga)Se_2 thin film solar cells, *Thin Solid Films*, 387 (2001) p. 29-32.
36. C. Platzer-Björkman, J. Lu, J. Kessler and L. Stolt, Interface study of Cu-$InSe_2$/ZnO and Cu(In,Ga)Se_2/ZnO devices using ALD ZnO buffer layers, *Thin Solid Films*, 431-432 (2003) p. 321-325.
37. J. Malmström, On Generation and Recombination in Cu(In,Ga)Se_2 Thin-Film Solar Cells, Ph.D. Thesis, Department of Engineering Sciences, 2005, Uppsala University, Uppsala.
38. D. Skoog, F. Holler and T. Nieman, Principles of Instrumental Analysis, fifth edition, 1998, Harcourt Brace and Company: New York.
39. M. Birkholz, Thin Film Analysis by X-Ray Scattering, 2006, WILEY-VCH verlag GmbH and Co. KGaA: Weinheim.
40. J. Moulder, W. Stickle, P. Sobol and K. Bomben, Handbook of X-ray Photoelectron Spectroscopy, 1995, Physical Electronics, Inc.: Eden Prairie, Minnesota.
41. J. Goldstein, D. Newbury, P. Echlin, D. Jpy, C. Fiori and E. Lifshin, Scanning Electron Microscopy and X-Ray Microanalysis, 1981, Plenum Press: New York.
42. L. Reimer, Transmission Electron Microscopy: Physics of Image Formation and Microanalysis, 4th Ed., 1997, Sprinerg-Verlag Berlin Heidelberg: New York.
43. W. Chu, J. W. Mayer and M. Nicolet, Backscattering spectrometry, 1978, Academic Press: New York.
44. H. Fritzsche, The Hall Effect, in: K. Lark-Horovitz and V. Johnson (Eds.), Methods of Experimental Physics, Volume 6, Solid State Physics, Part B: Electrical, Magnetic and Optical Properties, 1965, Academic Press Inc. Ltd.: London.
45. C. Platzer-Björkman, T. Törndahl, D. Abou-Ras, J. Malmström, J. Kessler and L. Stolt, Zn(O,S)/Cu(In,Ga)Se_2 solar cells: band alignment and sulfur gradient, *Journal of Applied Physics*, 100 (2006) p. 044506-1-9.
46. C. Persson, C. Platzer-Björkman, J. Malmström, T. Törndahl and M. Edoff, Strong Valence-band offset bowing of $ZnO_{1-x}S_x$ enhances p-type nitrogen doping of ZnO-like alloys, *Physical Review Letters*, 97 (2006) p. 146403-1-4.
47. U. Rau and H. Schock, Cu(In,Ga)Se_2 solar cells, in: M. Archer, R. Hill (Eds.), Clean Electricity From Photovoltaics, Volume 1, 2001, Imperial College Press: London.
48. U. Malm, J. Malmström, C. Platzer-Björkman and L. Stolt, Determination of dominant recombination paths in Cu(In,Ga)Se_2 thin-film solar cells with ALD-ZnO buffer layers, *Thin Solid Films*, 480-481 (2005) p. 208-212.
49. M. Contreras, B. Egaas, D. King, A. Swartzlander and T. Dullweber, Texture manipulation of $CuInSe_2$ thin films, *Thin Solid Films*, 361-362 (2000) p.167-171.

50. T. Törndahl, C. Platzer-Björkman, J. Kessler and M. Edoff, Atomic Layer Deposition of $Zn_{1-x}Mg_xO$ buffer layers for Cu(In,Ga)Se_2 solar cells, *Progress in Photovoltaics: Research and Applications*, 15 (2006) p. 225-235.
51. T. Minemoto, Y. Hashimoto, T. Satoh, T. Negami, H. Takakura and Y. Hamakawa, Cu(In,Ga)Se_2 solar cells with controlled conduction band offset of window/Cu(In,Ga)Se_2 layers, *Journal of Applied Physics*, 89 (2001) p. 8327-8330.
52. N. Allsop, C. Camus, S. Gledhill, T. Unold, M. Lu-Stiener, T. Niesen and C.-H. Fischer, Nanostructured ZnS:In_2S_3 buffer layers on Cu(In,Ga)$(S,Se)_2$: can voltage and efficiency be improved through interface inhomogenities on a scale below the minority carrier diffusion length, *Materials Research Symposium Proceedings*, Spring meeting, San Francisco, 1012 (2007) p. 43-49.
53. S. Chaisitsak, T. Sugiyama, A. Yamada and M. Konagai, Cu(In,Ga)Se_2 thin-film solar cells with high resistivity ZnO buffer layers deposited by atomic layer deposition, *Japanese Journal of Applied Physics*, Part 1, 38 (1999) p. 4989-4992.
54. D. Redfield and R. Bube, Photoinduced Defects in Semiconductors, 1996, Cambridge University Press, Cambridge.
55. D. Lang and R. Logan, Large-Lattice-Relaxation Model for Persistent Photoconductivity in Compound Semiconductors, *Physical Review Letters*, 39 (1977) p. 635-639.
56. D. Lang, J. Lau and M. Jaros, Tapping characteristics and donor-complex (DX) model for the persistent-photoconductivity tapping center in Te-doped $Al_xGa_{1-x}As$, *Physical Review B*, 19 (1979) p. 1015-1030.
57. T. Minemoto, H. Hori and H. Takakaura, Light soaking effect on photocurrent collection in (Zn,Mg)O/Cu(In,Ga)Se_2 solar cells, *Physica Status Solidi C*, 6 (2009) p. 1225-1228.
58. D. Hariskos, R. Herberholz, M. Ruckh, R. Schäffler and H. Schock, Buffer Layers for Cu(In,Ga)$(Se,S)_2$/BF/ZnO Solar Cells, *Proceedings of the 13th European Photovoltaic Energy Conference*, Nice, (1995) p. 1995-1999.
59. C. Platzer-Björkman, J. Kessler and L.Stolt, Atomic Layer Deposition of Zn(O,S) buffer layers for high efficiency Cu(In,Ga)Se_2 solar cells, *Proceedings of the 3rd World Conference on Photo-voltaic Energy Conversion*, Osaka, 1 (2003) p.461-464.
60. C. Platzer-Björkman, P. Zabierowski, J. Pettersson, T. Törndahl and M. Edoff, Improved fill factor and open circuit voltage by crystalline selenium at the Cu(In,Ga)Se_2/buffer layer interface in thin film solar cells, *Progress in Photovoltaics: Research and Applications*, 18 (2010) p. 249-256.
61. D. Hariskos, B. Fuchs, R. Menner, M. Powalla, N. Naghavi and D. Lincot, The ZnS/ZnMgO buffer combination in CIGS-based solar cells, *Proceedings of the 22nd European Photovoltaic Energy Conference and Exhibition*, Milan, (2007) p. 1907-1910.
62. T. Minemoto, Y. Hashimoto, W. Shams-Kolahi, T. Satoh, T. Negami, H. Takakura and Y. Hamakawa, Control of conduction band offset in wide-gap Cu(In,Ga)Se_2 solar cells, *Solar Energy Materials and Solar Cells*, 75 (2003) p. 121-126.

Acta Universitatis Upsaliensis

Digital Comprehensive Summaries of Uppsala Dissertations from the Faculty of Science and Technology 717

Editor: The Dean of the Faculty of Science and Technology

A doctoral dissertation from the Faculty of Science and Technology, Uppsala University, is usually a summary of a number of papers. A few copies of the complete dissertation are kept at major Swedish research libraries, while the summary alone is distributed internationally through the series Digital Comprehensive Summaries of Uppsala Dissertations from the Faculty of Science and Technology. (Prior to January, 2005, the series was published under the title "Comprehensive Summaries of Uppsala Dissertations from the Faculty of Science and Technology".)

Distribution: publications.uu.se
urn:nbn:se:uu:diva-133112

ACTA
UNIVERSITATIS
UPSALIENSIS
UPPSALA
2010